

國立交通大學

電子工程學系 電子研究所碩士班

碩 士 論 文

適用於多重輸入多重輸出正交分頻多工之二階統計特

性預先編碼盲式等化器

Second-Order Statistics Based

Precoder-Blind Equalization for MIMO-OFDM

學生：郭冠麟

指導教授：李鎮宜 教授，馮智豪 教授

中華民國九十七年七月

適用於多重輸入多重輸出正交分頻多工之二階統計特
性預先編碼盲式等化器

**Second-Order Statistics Based
Precoder-Blind Equalization for MIMO-OFDM**

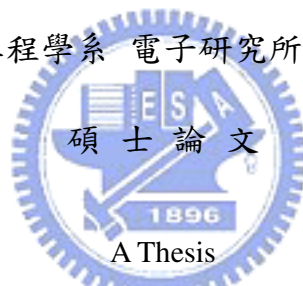
研究生：郭冠麟

Student : Kuan-Ling Kuo

指導教授：李鎮宜, 馮智豪 Advisor : C.-Y. Lee, C. C. Fung

國立交通大學

電子工程學系 電子研究所 碩士班



Submitted to Department of Electronics Engineering & Institute of Electronics
College of Electrical and Computer Engineering
National Chiao Tung University
in Partial Fulfillment of the Requirements
for the Degree of
Master of Science
in
Electronics Engineering

July 2008

Hsinchu, Taiwan, Republic of China

中華民國九十七年七月

適用於多重輸入多重輸出正交分頻多工之二階統計特性 性預先編碼盲式等化器

學生：郭冠麟 指導教授：李鎮宜 教授， 馮智豪 教授

國立交通大學

電子工程學系 電子研究所碩士班



摘要

許多通道效應，諸如路徑衰減、遮蔽效應，以及多重路徑衰減等等，已知會對無線通訊系統的效能造成破壞。特別對於多載波系統而言，多重路徑衰減會引起符號間干擾和載波間干擾而嚴重破壞傳輸的穩定性。與通道雜訊不同的是，符號間干擾和載波間干擾所造成的位元錯誤率，無法透過簡單地升高訊雜比加以解決。因此，通道等化時常成為必需步驟以減少此類不良影響。

傳統的等化程序包含了兩個步驟：通道估計與通道等化。首先，序言符號和導引符號等大量的訓練符號被應用於估計通道；等化器便可根據通道估計加以設計。然而，由於大量訓練符號的使用，頻譜效率無疑將減少。除此之外，當通道為快速衰減時，將需要傳送更多的導引符號，進一步地消耗稀少的傳輸資源。隨著高資料傳輸率的需求成長，此類型的傳輸代價將成為未來通訊系統的瓶頸。

在此篇論文中，一個適用於多重輸入多重輸出多頻分工系統的二階統計特性預先編碼盲式等化器被提出以減輕此類傳輸代價。被提出的技術可以等化有限脈衝響應的多重輸入多重輸出通道，並且不需要一個獨立的通道估計步驟。相較於

兩步驟的等化程序，這是一個優點。因為通道估計誤差可能在等化器設計時不被考慮，造成等化器的設計未被最佳化。所提出的架構在傳送端使用了正交預先編碼器，以滿足傳送訊號必須是時間相關的可辨別條件。此外，編碼器被設計為可減少接收端等化器的時間延遲和計算複雜度。在位元錯誤率與計算複雜度方面，此架構能優於先前提出的二階統計特性預先編碼盲式等化器。模擬結果顯示，位元錯誤率的效能也逼近一個有理想通道資訊的最小平方迫零法等化器。模擬結果也顯示，所提出系統在 10 根天線與訊雜比 10dB 的情況下，通道容量可達到 25 bits/s/Hz 以上。



Second-Order Statistics Based Precoder-Blind Equalization for MIMO-OFDM

Student : Kuan-Ling Kuo

Advisor : C.-Y. Lee, C. C. Fung

Department of Electronics Engineering and Institute of
Electronics,
National Chiao Tung University



Channel effects such as path loss, shadowing, and multipath fading have been known to hamper performance of wireless communication systems. In particular, multipath fading causes intersymbol interference (ISI) and intercarrier interference (ICI) in the case of multicarrier systems, if it is not handled properly, can severely degrade link reliability. Unlike additive channel noise, BER degradation from ISI and ICI cannot be prevented by simply increasing the SNR. Hence, channel equalization is often necessary in order to mitigate these detrimental effects.

Conventional equalization procedure usually involves two steps which includes channel estimation followed by equalization. Large number of training symbols, such as preambles and pilots, are first used to identify the channel. An equalizer can then be designed using the channel estimate. However, spectral efficiency will undoubtedly

be decreased due to the use of these training signals. Furthermore, when the channel is undergoing fast fading, even more pilot symbols are needed to be sent; further consuming scarce transmission resources. With the growing demand for higher data rate, this type of transmission overhead will be a bottleneck for future communication systems.

In this thesis, a second-order statistics based precoder-blind equalizer for MIMO-OFDM system is proposed to alleviate the problems of transmission overhead. The proposed technique can equalize FIR-MIMO channels directly without an explicit channel estimation step. This is an advantage over the traditional two-step approach, where the channel is first estimated followed by the design of the equalizer coefficients, because the second step will likely result in a suboptimal equalizer since errors in the channel estimates are not taken into account. The proposed scheme uses a set of orthogonal precoders at the transmitter such that the transmitted signal can be colored temporally thereby satisfying the identifiability condition previously proposed by Hua and Tugnait. Moreover, the precoders are designed to reduce latency and computational complexity of equalization at the receiver. The scheme is shown to outperform previously proposed SOS-based precoder-blind equalization schemes in terms of BER and computational complexity. Simulation results have shown that the BER performance is close to that of a least-squares zero-forcing equalizer with perfect channel knowledge. Simulation results have also shown that the capacity of the proposed scheme can be above 25 bits/s/Hz while 10 antennas are exploited at SNR of 10 dB.

Acknowledgement

Thanks Profs. Chen-Yi Lee and Carrson C. Fung for inspiring me to see the possible ways throughout the journey of my study, giving valuable guidance to integrate my thinking and providing abundant resources during the past two years. Thanks to them, I was able to develop the research skills to undertake and complete this work.

I also like to thank my lab-mates, Jui-Yuan Yu and Tsan-Wen Chen, for their great help to me. They were necessary companions for this thesis to come into being.



Contents

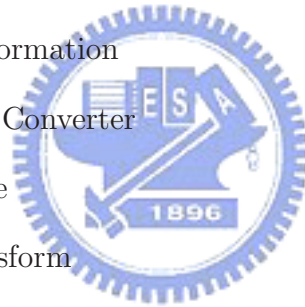
1	Introduction	1
1.1	Research Motivation	1
1.2	Thesis Organization	5
1.3	Publications	6
2	Fundamentals of MIMO-OFDM Systems	7
2.1	OFDM System Model	7
2.2	MIMO-OFDM Systems Model	11
2.2.1	Concept of MIMO System	12
2.2.2	MIMO-OFDM Model	17
2.3	Frame Format	19
3	Precoder-Blind Equalization Algorithm for MIMO-OFDM	21
3.1	SOS-Based Blind Identifiability and Equalizability Conditions for FIR-MIMO Systems	21
3.1.1	Identifiability Conditions	21
3.1.2	Equalizability Conditions	22
3.2	SOS-Based Blind Channel Identification and Equalization	23
3.2.1	Existing SOS-Based Periodic Precoding Channel Identification	23
3.2.2	SOS-Based Precoder-Blind Equalization	29

3.3	Precoder Design	33
3.3.1	Precoder Format	33
3.3.2	Temporal Correlation Injection	36
3.4	Results and Discussions	39
3.4.1	Computational Complexity	39
3.4.2	Implementation of Precoders by Memory-Based IFFT/FFT	40
3.4.3	BER performance	45
3.4.4	Channel Capacity	54
4	Conclusion and Future Work	56
4.1	Conclusion	56
4.2	Future Work	57



Abbreviations and Notations

ADC	Analog-to-Digital Converter
AWGN	Additive White Gaussian Noise
BER	Bit Error Rate
CFO	Carrier Frequency Offset
CP	Cyclic Prefix
CSI	Channel State Information
DAC	Digital-to-Analog Converter
DMT	Discrete Multitone
FFT	Fast Fourier Transform
FIR	Finite Impulse Response
HOS	Higher-Order Statistics
ICI	Intercarrier Interference
IFFT	Inverse Fast Fourier Transform
ISI	Intersymbol Interference
JD	Joint Diagonalization
LOS	Line-Of-Sight
LS	Least-Squares
LTI	Linear Time Invariant
MIMO	Multiple-Input and Multiple-Output
OFDM	Orthogonal Frequency-Division Multiplexing



PAPR	Peak-to-Average-Power Ratio
QPSK	Quadrature Phase Shift Keying
SCO	Sampling Clock Offset
SIMO	Single-Input and Multiple-Output
SISO	Single-Input and Single-Output
SNR	Signal-to-Noise Ratio
SOS	Second-Order Statistics
STBC	Space-Time Block Code
STC	Space-Time Code
STO	Sampling Timing Offset
STTC	Space-Time Trellis Code

Notations: Upper (lower) bold face letters indicate matrices (column vectors). Superscript H denotes Hermitian, T denotes transposition. $E[\cdot]$ stands for expectation. $diag(x)$ denotes a diagonal matrix with x on its main diagonal; \mathbf{I}_N denotes an $N \times N$ identity matrix; $\mathbf{0}_{M \times N}$ denotes an $M \times N$ all zero matrix.

List of Figures

2.1	Simplified block diagram of OFDM systems	8
2.2	Cyclic prefix of an OFDM symbol	8
2.3	Spectrum of an OFDM symbol	9
2.4	A transmitter of the OFDM system	10
2.5	A receiver of the OFDM system	10
2.6	A block diagram of the Alamouti space-time encoder	13
2.7	Schematic of the generic MIMO system	14
2.8	MIMO-OFDM system	20
3.1	Block diagram of equalization process with 2 receive antennas where JD represents joint diagonalization.	31
3.2	The transmitter of the precoder-blind equalizer system with 2 Tx/Rx antennas.	34
3.3	The receiver of the precoder-blind equalizer system with 2 Tx/Rx antennas.	35
3.4	A typical memory-based FFT architecture [36].	42
3.5	Spectrum of the coloring precoders.	45
3.6	Comparison of BER performance between system without coloring and with coloring for 3-tap channel.	46
3.7	BER vs. different number of received OFDM symbols for 3-tap channel at SNR = 10, 14, 18 dB.	47

3.8	Comparison of BER vs. SNR with different algorithms for 3-tap channel.	50
3.9	Comparison of BER vs. SNR with different algorithms for 7-tap channel.	50
3.10	BER vs. SNR with different lag for 3-tap channel.	51
3.11	BER vs. SNR with different P for 3-tap channel.	53
3.12	BER vs. SNR with different γ for 3-tap channel.	53
3.13	Capacity vs. Number of antennas with different SNR.	55
3.14	Capacity per n vs. SNR with different n	55



List of Tables

2.1	Summary of frame format	19
3.1	Values for C_{i,τ_p} for $L + q > N_t P$	38
3.2	Values for C_{i,τ_p} for $L + q \leq N_t P$	38
3.3	Values for C_{i,τ_p} when $q = 2, L = 2, P = 2, N_t = 2$	39
3.4	Performance comparison	49



Chapter 1

Introduction

1.1 Research Motivation

In general communication environments, many surrounding objects such as vehicles, building or trees may act as reflectors of transmitted signal. Reflected waves are produced with attenuated amplitude by these obstacles and arrive at the receiver from various directions with different delays. The sum of these multiple reflected waves forms the multipath channel, which causes various forms of distortion on the transmitted signal. For a narrowband system, the transmitted signal usually occupies a bandwidth smaller than the coherence bandwidth of channels. Therefore, all spectral components of the transmitted signal experience the same fading during transmission. This class of fading channel is called frequency flat, which requires no equalization since the fading attenuation is fixed over the entire transmission. However, with the insatiable need to transmit more data at any time and anywhere, next generation wireless communication systems, such as IEEE 802.11n and 802.16m, are required to support higher data rate than their predecessors, while the mobile terminals are undergoing faster mobility. To deliver systems that can operate reliably under such harsh conditions, researchers have also focused their attention on the wireless broadband communications systems, which aim to offer multimedia services

requiring data rates beyond 2 Mbps. This can be achieved by increasing the sampling rate of the information bearing signal. However, this will likely cause the bandwidth of the transmitted signal to be larger than the coherence bandwidth of the channel, which distorts the spectrum of the transmitted signal differently at different frequencies and causes ISI in the time domain. In this case, the channel is said to be frequency selective fading.

Since its invention in the 1980s [1], OFDM has become the method of choice for high data rate transmission over frequency selective fading channels. One of the major advantages of OFDM is that it can completely equalize (assuming accurate CSI) a frequency selective fading channel with relatively low computational complexity compared to other signaling schemes. This can be achieved as long as the length of the CP is not less than the order of the fading channel.

Data rate and link reliability can be increased through the use of MIMO techniques which have been recently proposed in the literature [2,3]. Analytic and simulation results have shown that system capacity and link reliability can be dramatically improved by means of spatial multiplexing and spatial diversity, respectively. Spatial multiplexing can be achieved by methods such as VBLAST [4] or linear precoding [5]. In the latter approach, the source data is split into multiple data streams and precoded by a precoder matrix, such as the right singular vector matrix of the channel, before each stream is launched to a different transmit antenna. When the data arrive at the receiver, the receiver can recover the transmitted signal by simply multiplying the signal by the left singular vector matrix of the channel, followed by multiplication of the singular values of the channel. Therefore, the maximum number of data streams is limited by $\min(N_t, N_r)$, where N_t and N_r denote the number of transmit and receive antennas, respectively. On the other hand, spatial diversity is achieved when a single data stream is transmitted using multiple antennas with the assumption that there is negligible spatial correlation

among the transmit and receive antennas. It has been shown that techniques such as STTC and STBC can be used to achieve full diversity order, but at the expense of lower code rate or increase computational complexity. The motivation is that the signal will undergo independent fading in different spatial channels such that even if one signal is corrupted, it is unlikely that its duplicates will be similarly distorted; allowing recovery of the transmitted signal to be possible.

Recently, a vast amount of literature has been devoted to the study of MIMO-OFDM systems; with the hope that the marriage of the two technologies can increase system performance without incurring a large penalty in terms of computations for broadband communication systems [6]. However, large transmission overhead in the form preamble, signal pilot and guard interval severely hamper the performance of such systems. For example, in the IEEE 802.16-2004 standard, widely known as fixed WiMAX, it was shown in [7] that the overhead introduced by the physical layer alone can be more than 50%. This has made blind channel estimation and equalization techniques for MIMO-OFDM systems an attractive alternative because of their ability to increase capacity of MIMO communication systems without sacrificing spectral efficiency [8,9].

Traditionally, blind channel estimation and equalization has been based on HOS of the received signal [10,11]. Although these schemes are technically different, most of them apply higher-order cumulants of the observation to optimize certain criteria in order to identify the zeros of a nonminimum phase system, however, under many strict conditions of transmitted signal. Higher-order whiteness and higher-order weak stationarity of transmitted signal are both required for the exploitation of higher-order cumulants. Furthermore, the estimates of HOS usually converge slower than those of SOS such that more received symbols are required. Hence, much of the research effort has shifted toward using SOS after the seminal work by [12] and [13] since SOS based techniques can also estimate and equalize nonminimum phase FIR channels at much lower latency than its HOS

counterparts. SOS based techniques can basically be categorized into either deterministic or statistics based approach. A deterministic approach was proposed in [13] to estimate FIR-SIMO channels. In this case, the system input is treated as an arbitrary unknown deterministic signal. The basic idea is to exploit commutability of the convolution operator using $h_k[n] * x_j[n] = h_j[n] * x_k[n]$, where $h_k[n]$ and $x_k[n]$ denote the channel impulse response from the transmit antenna to the k^{th} receive antenna and the received signal of the k^{th} receive antenna, respectively. For each pair of (k, j) , a set of linear equations can be given to solve the channel responses. A statistical approach for oversampled FIR-SISO systems is presented in [12]. The cyclostationarity of the received signal is used to identify channels via oversampling, and the channel matrix is assumed to have full column rank. The correlation matrices with lag equal to 0 and 1 are both required. The noise power estimation is therefore demanded since the estimation of the correlation matrix with lag equal to 0 is contaminated by channel noise. These previous results have led to the work by [14] which exploited the subspace method to estimate FIR-SIMO channels. Good performance in terms of mean squared error (MSE) can be achieved in high SNR condition. However, its performance degrades at a fast rate in low SNR condition, such as 0 – 10 dB. An FIR-MIMO extension of the subspace method was proposed in [15, 16] which suffers from the same problem as its SIMO counterpart in low SNR condition. The subspace channel estimation method requires the channel transfer function matrix, $\mathbf{H}(z)$, to be *irreducible* and *column-reduced* [17], which limited the application of SOS based methods to a narrow class of communication channels.

Recently, [18] has shown that a weaker condition for the identifiability of $\mathbf{H}(z)$ exists, where $\mathbf{H}(z)$ can be identified up to scaling and permutation ambiguity if $\mathbf{H}(z)$ is *irreducible* and the power spectral density matrix of the channel input signal is a diagonal matrix with distinct diagonal functions. [19] has proposed an algorithm for estimating $\mathbf{H}(z)$ under this weaker condition, but a direct equalization algorithm was never discussed. [20]

has proposed a SOS based blind equalization algorithm which implicitly uses the identifiability conditions stated in [18] for flat fading channels, where the number of transmit antennas, N_t , has to be equal to the number of receive antennas, N_r . [21] also exploited this condition by designing a novel SOS based channel estimation algorithm to estimate MIMO channels for OFDM based systems. The algorithm uses cyclic power spectral density of the received signal to decouple the MIMO channels into parallel SISO channels for estimation. The technique requires the use of a precoder to inject cyclostationarity into the input bitstream. Although not stated in [21], but the precoder actually colors the signal such that MIMO channel equalization using SOS is possible. [22] has extended the SOS algorithm in [20] such that any FIR-MIMO channel $\mathbf{H}(z)$ can be equalized up to a scaling, phase, and block delay ambiguity given that the identifiability conditions in [18] are satisfied. This was accomplished by designing the blind FIR equalizer within the space-time precoder-equalizer system where redundancy is injected into the transmitted bitstream to make FIR-MIMO channel equalization possible using an FIR equalizer. In [22], the independently distributed input signal streams were colored using a set of low complexity filters to satisfy the power spectral density condition stated in [18] such that the algorithm in [20] can be extended to be applicable to ISI channels and general space-time systems. However, the precoder that was proposed was not optimally designed. As shown in the Section 3.4, this not only impacts the equalization performance, but also increases the computational complexity at the receiver.

1.2 Thesis Organization

In this thesis, we extended the precoder-blind equalization scheme to MIMO-OFDM spatial multiplexing system, and proposed a new set of precoder to perform direct channel equalization for MIMO-OFDM systems such that improved BER performance and lower receiver complexity can be achieved compared to that of [22]. In Chapter 2, we will

give a description of the system model for MIMO-OFDM, followed by a review of blind identification conditions, blind equalization conditions and the equalization algorithms in Chapter 3. A novel precoder design and a blind equalizer for MIMO-OFDM are proposed in Chapter 3, which directly equalize an MIMO-OFDM channel blindly without an explicit channel estimation step. Simulation results will show that the proposed algorithm has lower or comparable performance as other SOS-based algorithms but with less computational complexity. The conclusion and future work will be discussed in Chapter 4.

1.3 Publications

Conference:

Kuan-Ling Kuo, Tsan-Wen Chen, Carrson C. Fung and Chen-Yi Lee, Second-Order Statistics Based prefilter-Blind Equalization for MIMO-OFDM, *to be presented at the 14th Asia-Pacific Conference on Communications*, Oct. 2008.

Journal:

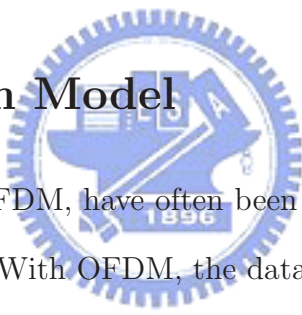
Kuan-Ling Kuo, Tsan-Wen Chen, Carrson C. Fung and Chen-Yi Lee, Second-Order Statistics Based Precoder-Blind Equalization for MIMO-OFDM, *in preparation*.

Chapter 2

Fundamentals of MIMO-OFDM

Systems

2.1 OFDM System Model



Multicarrier systems, such as OFDM, have often been used to combat against frequency selective fading channel effects. With OFDM, the data is transmitted in various narrow-band orthogonal channels. This is accomplished easily by the use of IFFT and FFT to modulate and demodulate the signal. A simplified block diagram of OFDM is shown in Figure 2.1, where f_k denotes the subcarrier and $\tilde{\eta}(n)$ is the channel noise. On one hand, IFFT and FFT are efficient in terms of spectrum usage and implementation because only one pair of oscillators for the I- and Q-path is required by the RF front-end instead of multiple oscillators to modulate different paths at different carriers. When the transmitted signal passes through the channel, ISI and ICI usually occur. CP is hence introduced to combat ISI and ICI. The CP, shown in Figure 2.2, is a copy of the tail part of a OFDM symbol, which is inserted between the current symbol and its preceding symbol. As long as the length of the CP is not less than the order of the fading channel, ISI can be avoided. This can be explained by noting the channel matrix, with the addition of the

CP of sufficient length, is now a circulant matrix such that it can always be diagonalized by a FFT matrix. Consequently, the frequency selective fading channel has now been converted into a frequency flat fading channel.

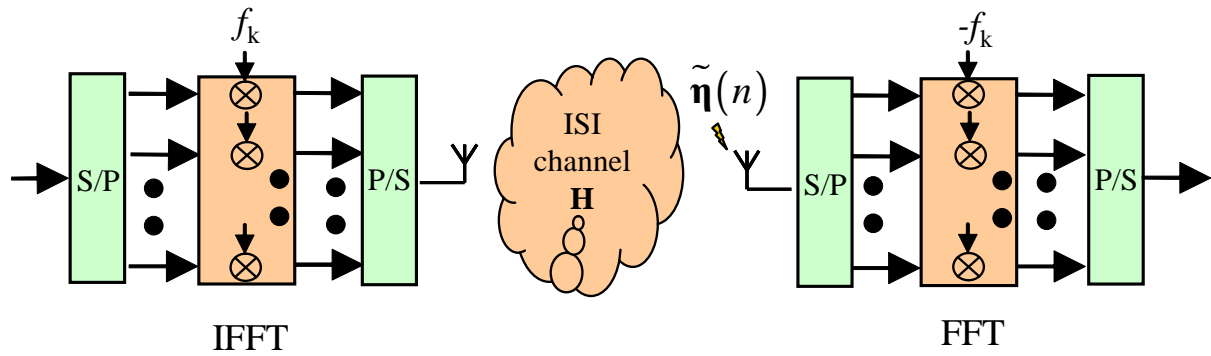


Figure 2.1: Simplified block diagram of OFDM systems

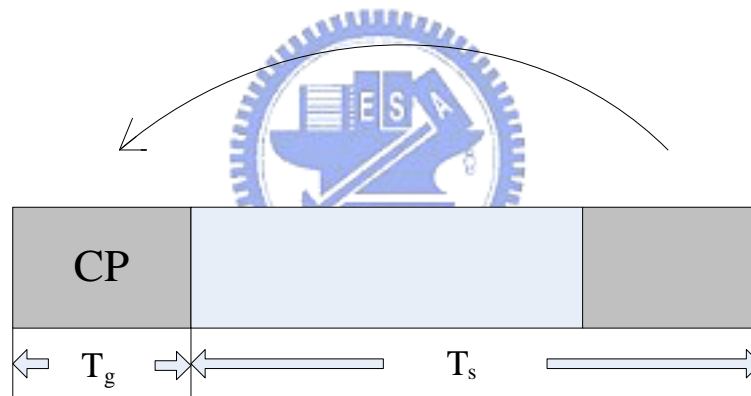


Figure 2.2: Cyclic prefix of an OFDM symbol

With all its strengths, OFDM-based systems do suffer from problems such as high PAPR and high sensitivity to frequency synchronization. High PAPR is possible since the linear summation of independent phases from all subcarriers often lead to a constructive combination. A DAC and an ADC with high resolution, which result in large hardware complexity and cost, are thereby needed to transmit OFDM signal with high PAPR. Linearity range of power amplifiers is also required to be large to prevent saturation. This undoubtedly leads to the use of expensive linear power amplifier. In fact, a small amount

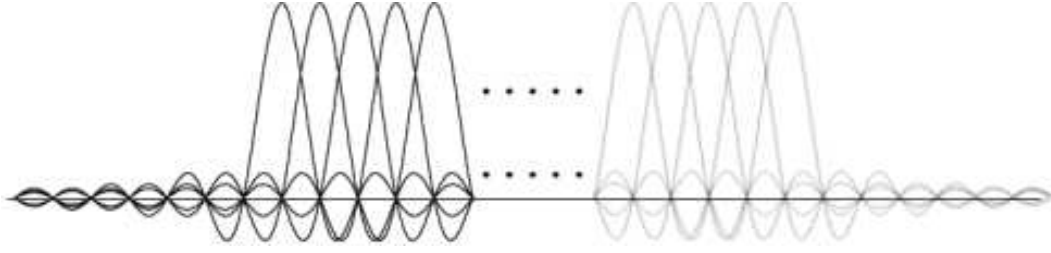


Figure 2.3: Spectrum of an OFDM symbol

of peak clipping is usually allowed to limit the PAPR [23]. Moreover, nonideal effects of frequency synchronization such as SCO, STO and CFO will also degrade performance of OFDM-based systems because they will induce ICI and ISI into the system.

Since the modulation and demodulation of OFDM are implemented efficiently by using IFFT and FFT operation, respectively, the output of the IFFT is given by

$$\begin{aligned}
 u[n] &= \sum_{m=0}^{M-1} s[m] e^{j \frac{2\pi}{M} mn} \\
 &= \sum_{m=0}^{M-1} s[m] \phi_m[i],
 \end{aligned}$$

where $s[m]$ is the source data in the m^{th} path. Similarly, the output of the FFT is given as

$$\begin{aligned}
 y[n] &= \sum_{m=0}^{M-1} x[m] e^{-j \frac{2\pi}{M} mn} \\
 &= \sum_{m=0}^{M-1} x[m] \psi_m[i],
 \end{aligned}$$

where $x[m]$ is the received data in the m^{th} path. M is the IFFT/FFT size.

Figure 2.4 and Figure 2.5 show the transmitter with CP insertion and receiver with CP removal of an OFDM system, respectively. At the transmitter, the IFFT transforms source data from frequency-domain into time-domain. After a parallel-to-serial conversion, the CP is inserted to the information bearing signal before it is delivered over the channel. At the receiver, CP is first removed followed by FFT demodulation. Assumed the given channel is constant during the transmission of an OFDM symbol, the received signal $x[n]$

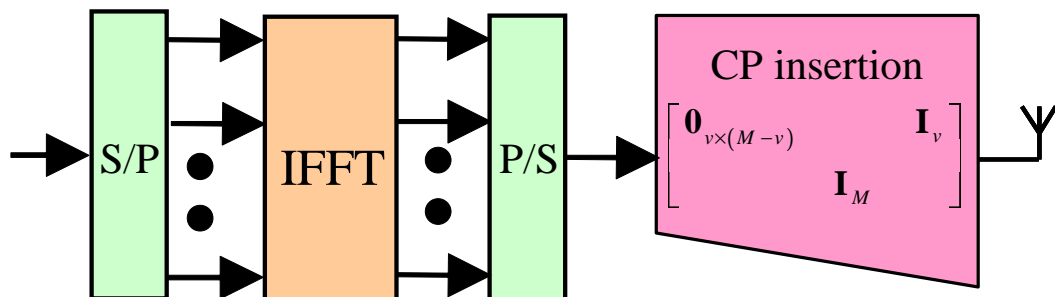


Figure 2.4: A transmitter of the OFDM system

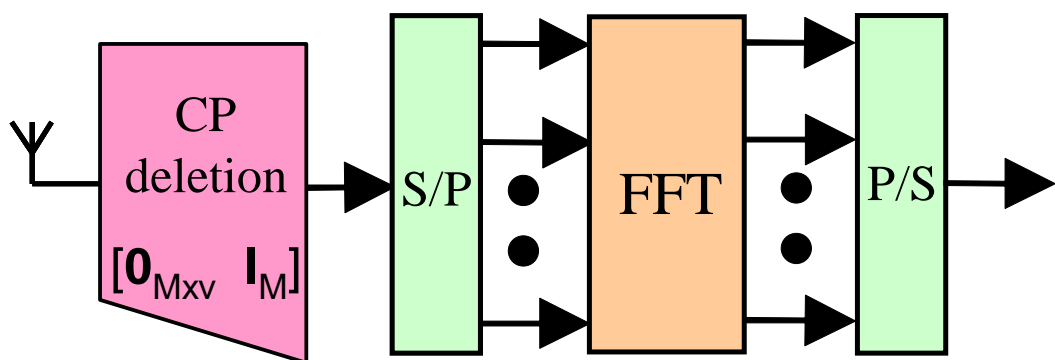


Figure 2.5: A receiver of the OFDM system

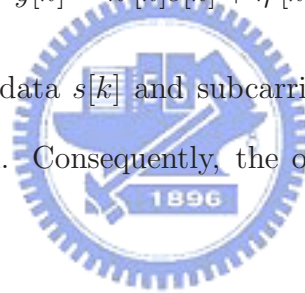
can be expressed as

$$x[n] = u[n] * h[n] + \eta[n],$$

where $u[n]$ is the transmitted data, $\eta[n]$ represents the channel noise, $h[n]$ denotes the channel impulse response, and $*$ denotes linear convolution. Because of multipath channels, orthogonality as shown in Figure 2.3 will be destroyed by ISI and ICI. However, as long as the length of the CP is not less than the order of $h[n]$, ISI effect can be avoided. At the same time, linear convolution of $u[n]$ and $h[n]$ will become circular convolution because of the insertion of CP. It is known that circular convolution in time domain results in multiplication in frequency domain when the channel is stationary. The demodulated signal $y[k]$ in frequency domain at the receiver can then be written as

$$y[k] = h'[k]s[k] + \eta'[k],$$

which is the product of source data $s[k]$ and subcarrier channel response $h'[k]$ plus the noise $\eta'[k]$ in frequency domain. Consequently, the orthogonality among subcarriers is maintained without ICI.



2.2 MIMO-OFDM Systems Model

The quality of a wireless link can be measured by three metrics: the transmission rate, the transmission range and the transmission reliability. Conventionally, the transmission rate may be increased by reducing the transmission range and reliability. By contrast, the transmission range may be extended at the cost of a lower transmission rate and reliability, while the transmission reliability may be improved by reducing the transmission rate and range [24]. However, with the advent of MIMO-OFDM systems, the three metrics mentioned above may be simultaneously improved as described in [24]. MIMO-OFDM communication systems have shown that an increased capacity, coverage and reliability is achievable with the aid of MIMO techniques. Although MIMO techniques can potentially

be combined with any other modulation or multiple access schemes, MIMO-OFDM has attracted extensive research because high spectral efficiency and high reliability can be obtained with relatively low computational complexity.

2.2.1 Concept of MIMO System

MIMO is a technology which exploits the rich scattering environment at the transmitter and/or receiver such that when multiple spatial data streams are launched into the channel, they will be distorted *independently* by the channel; thereby increasing the probability of recovering the transmitted data at the receiver. One of the motivation for MIMO is to significantly increase the data throughput without additional bandwidth or transmit power. This is achieved by taking advantages of the rich scattering environment surrounding the transmission terminal and by using spatial multiplexing, where a high-rate source data stream is split into multiple low rate data streams according to the number of transmit antennas. Each data stream is then emitted by a different transmit antenna in the same bandwidth. In a rich scattering environment, the transmitter is able to transmit the signal in parallel channels with distinguished non-zero eigenmode. The transmission from different transmit antennas are hence distinguished. Through spatial multiplexing, multiple data streams can be transmitted simultaneously over independent parallel channels, and therefore the transmission rate and capacity will be increased. Consequently, MIMO techniques are often applied for high speed broadband wireless communications.

Considering the trade-off between capacity and reliability, it is possible to increase the link reliability by the use of transmit diversity. If a single data stream is transmitted by multiple transmit antennas, several observations of the same stream will be obtained by multiple receive antennas. Under a rich scattering environment, the spatial diversity can be maximized for the fixed number of antennas. In this case, fading effects of channels are reduced such that the overall system becomes more reliable. STC techniques such as

STTC and STBC are usually applied to MIMO systems with transmit diversity. The basic idea of STC is transmitting multiple and redundant copies of a data stream to achieve transmit diversity. An example of STBC using Alamouti code [25] is shown in Figure 2.6, which has a simple two-branch transmit diversity. A block of two modulated symbols, u_1 and u_2 , is encoded by a coding matrix. The encoder outputs are then transmitted in

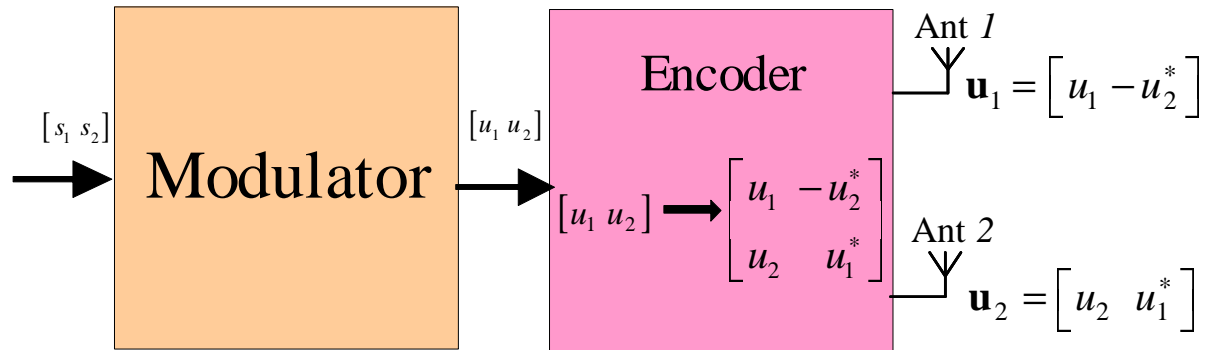


Figure 2.6: A block diagram of the Alamouti space-time encoder

two consecutive transmission periods from two transmit antennas, which are denoted as $\mathbf{u}_1 = [u_1 - u_2^*]$ and $\mathbf{u}_2 = [u_2 u_1^*]$, respectively. In the first transmission period, u_1 and u_2 are transmitted simultaneously from the first antenna and the second antenna, respectively. During the second period, $-u_2^*$ and u_1^* are transmitted from the first antenna and the second antenna, respectively. It is clear that the encoding involves with both space and time domains. Furthermore, the inner product of \mathbf{u}_1 and \mathbf{u}_2 is zero. In other words,

$$\mathbf{u}_1 \cdot \mathbf{u}_2 = u_1 u_2^* - u_2^* u_1 = 0,$$

such that the transmit sequences from two transmit antennas are orthogonal. The key feature of this scheme is that a full diversity gain can be achieved with a simple maximum-likelihood decoding algorithm at the receiver with perfect CSI. STBC with the number of transmit antennas greater than 2 based on orthogonal designs are discussed in [26]. Obviously, a trade-off between spatial multiplexing and spatial diversity for MIMO exists.

For a MIMO system with the fixed number of antennas, data rate and link reliability cannot be optimized simultaneously under the same channel [27].

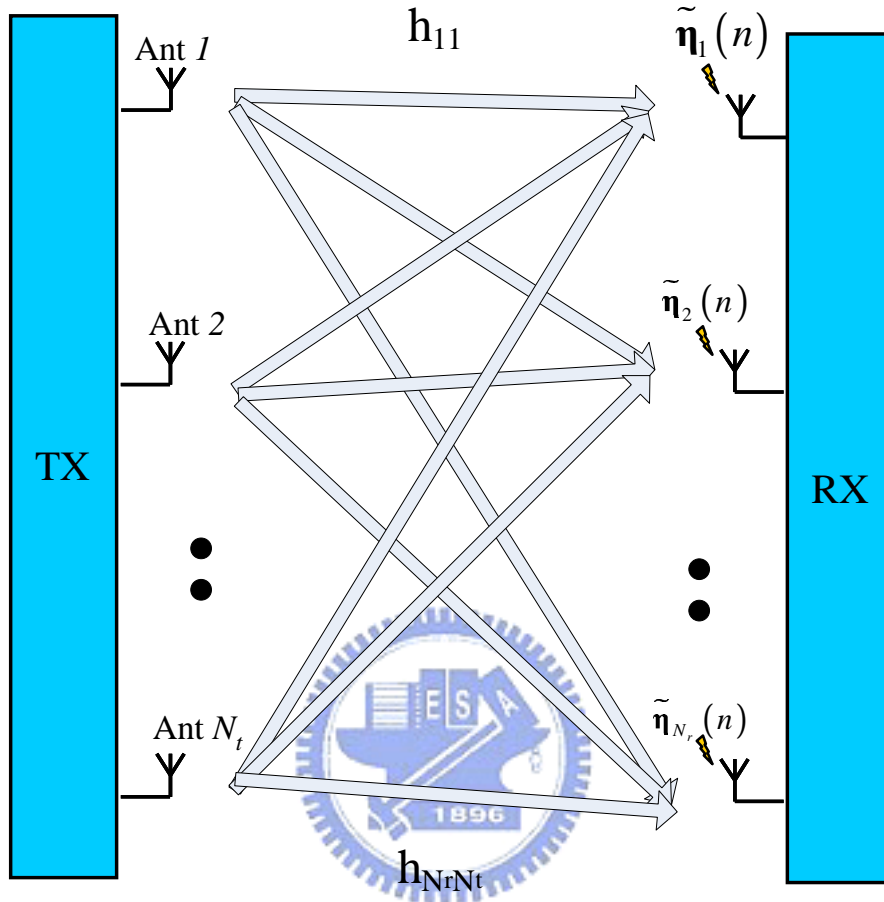


Figure 2.7: Schematic of the generic MIMO system

The schematic of a generic single-user MIMO system is illustrated in Figure 2.7, where N_t transmit antennas and N_r receive antennas are equipped at the transmitter and receiver, respectively. The following are conditions assumed for the MIMO system in Figure 2.7:

- The channel maintains invariant during the transmission of one frame, which means that channel is block or slow fading.
- The channel is frequency-flat fading, which means that spectrum of channel is constant over the whole bandwidth such that channel gain can be represented by a

complex number.

Under the above assumptions, the input/output relation of a narrowband, single-user MIMO system can be written as

$$\mathbf{x}[n] = \mathbf{H}\mathbf{u}[n] + \boldsymbol{\eta}[n],$$

where

$$\begin{aligned}\mathbf{x}[n] &= [x_1[n] \ x_2[n] \ \cdots \ x_{N_r}[n]]^T, \\ \mathbf{u}[n] &= [u_1[n] \ u_2[n] \ \cdots \ u_{N_t}[n]]^T, \\ \boldsymbol{\eta}[n] &= [\eta_1[n] \ \eta_2[n] \ \cdots \ \eta_{N_r}[n]]^T.\end{aligned}$$

$\mathbf{u}[n]$ is an $N_t \times 1$ transmit signal vector, $\mathbf{x}[n]$ is an $N_r \times 1$ receive signal vector, \mathbf{H} is the $N_r \times N_t$ channel matrix, and $\boldsymbol{\eta}[n]$ is the $N_r \times 1$ channel noise vector. The channel matrix is given as

$$\mathbf{H} = \begin{bmatrix} h_{11} & h_{12} & \cdots & h_{1N_t} \\ h_{21} & h_{22} & \cdots & h_{2N_t} \\ \vdots & \vdots & \ddots & \vdots \\ h_{N_r1} & h_{N_r2} & \cdots & h_{N_rN_t} \end{bmatrix},$$

where $h_{ij} = \alpha_{ij} + j\beta_{ij} = |h_{ij}|e^{j\phi_{ij}}$ represents the complex gain of the channel from the j^{th} transmit antenna to the i^{th} receive antenna. α_{ij} and β_{ij} are the real part and imaginary part of h_{ij} , respectively. ϕ_{ij} is the phase angle of h_{ij} and $|h_{ij}|$ is the magnitude. If α_{ij} and β_{ij} are independent and Gaussian distributed random variables, then $|h_{ij}|$ is Rayleigh distributed, which leads to a Rayleigh flat-fading channel.

While the transmission bandwidth is larger than the coherent bandwidth of channels, the channel is considered to be frequency selective. Denoting a frequency selective fading channel impulse response from the j^{th} transmit antenna to the i^{th} receive antenna as $\mathbf{h}_{ij} = [h_{ij}[0] \ h_{ij}[1] \ \cdots \ h_{ij}[q]]^T$, where q is the channel order. The $N_r \times N_t$ MIMO

matrix can then be written as

$$\mathbf{H}_\ell = \begin{bmatrix} h_{11}[\ell] & h_{12}[\ell] & \cdots & h_{1N_t}[\ell] \\ h_{21}[\ell] & h_{22}[\ell] & \cdots & h_{2N_t}[\ell] \\ \vdots & \vdots & \ddots & \vdots \\ h_{N_r1}[\ell] & h_{N_r2}[\ell] & \cdots & h_{N_rN_t}[\ell] \end{bmatrix},$$

where $\ell = 0, 1, \dots, q$. The input/output relation of the frequency selective fading channel can then be written as

$$\mathbf{x}[n] = \sum_{\ell=0}^q \mathbf{H}_\ell \mathbf{u}[n - \ell] + \boldsymbol{\eta}[n]. \quad (2.1)$$

Compared with frequency flat fading attenuation, (2.1) is a linear superposition of the product of \mathbf{H}_ℓ and the transmit signal vector due to convolution. (2.1) can be rewritten more compactly if we further define

$$\mathbf{H} \triangleq \begin{bmatrix} \mathbf{H}_0 & \mathbf{H}_1 & \cdots & \mathbf{H}_q & \mathbf{0} & \cdots & \cdots & \mathbf{0} \\ \mathbf{0} & \mathbf{H}_0 & \mathbf{H}_1 & \cdots & \mathbf{H}_q & \mathbf{0} & \cdots & \mathbf{0} \\ \vdots & \vdots & \vdots & \ddots & \vdots & \vdots & \ddots & \vdots \\ \mathbf{0} & \cdots & \cdots & \mathbf{0} & \mathbf{H}_0 & \mathbf{H}_1 & \cdots & \mathbf{H}_q \end{bmatrix}$$

and

$$\begin{aligned} \check{\mathbf{x}}[n] &\triangleq [\mathbf{x}^T[n] \quad \mathbf{x}^T[n-1] \quad \cdots \quad \mathbf{x}^T[n-L+1]]^T, \\ \check{\mathbf{u}}[n] &\triangleq [\mathbf{u}^T[n] \quad \mathbf{u}^T[n-1] \quad \cdots \quad \mathbf{u}^T[n-L-q+1]]^T, \\ \check{\boldsymbol{\eta}}[n] &\triangleq [\boldsymbol{\eta}^T[n] \quad \boldsymbol{\eta}^T[n-1] \quad \cdots \quad \boldsymbol{\eta}^T[n-L+1]]^T, \end{aligned}$$

where \mathbf{H} is an $N_r L \times N_t(L+q)$ MIMO frequency selective fading channel matrix. L is the number of the received signal vector. Using these definitions, the input/output relation in (2.1) can be written as

$$\check{\mathbf{x}}[n] = \mathbf{H}\check{\mathbf{u}}[n] + \check{\boldsymbol{\eta}}[n].$$

2.2.2 MIMO-OFDM Model

In this thesis, we shall consider a MIMO-OFDM system with N_t transmit antennas and N_r receive antennas as shown in Figure 2.8. A single transmit antenna is employed by each OFDM modulator including IFFT and CP insertion. Let $s_{m,\ell}^{(i)}$ denotes the complex-valued data symbol transmitted on the m^{th} tone in the ℓ^{th} OFDM symbol from the i^{th} transmit antenna for $i = 1, 2, \dots, N_t$. Also, let $K = M + v$ denote the overall OFDM symbol length, where M is the size of the IFFT/FFT and v is the length of the CP. Then the transmitted signal $u_i[n]$ after CP insertion can be written as [21]

$$u_i[n] = \sum_{\ell} g[n - \ell K] \sum_{m=0}^{M-1} s_{m,\ell}^{(i)} e^{j \frac{2\pi}{M} m(n - \ell K)},$$

where $g[n]$ is a rectangular function $rect_{[0, K-1]}[n]$ with

$$rect_{[T_1, T_2]}[n] = \begin{cases} 1, & n = T_1, T_1 + 1, \dots, T_2. \\ 0, & \text{otherwise.} \end{cases}$$

Then the received signal at the k^{th} receive antenna can be written as

$$x_k[n] = \sum_{i=1}^{N_t} \left[\sum_{\ell} h_{k,i}[\ell] u_i[n - \ell] \right] + \eta_k[n], \quad (2.2)$$

where $\eta_k[n]$, for $k = 1, 2, \dots, N_r$, is the stationary additive white channel noise at the k^{th} receive antenna and $h_{k,i}[\ell]$ is the discrete-time channel impulse response of the channel.

Defining

$$\begin{aligned} \mathbf{x}[n] &\triangleq [x_1[n] \ x_2[n] \ \cdots \ x_{N_r}[n]]^T, \\ \mathbf{u}[n] &\triangleq [u_1[n] \ u_2[n] \ \cdots \ u_{N_t}[n]]^T, \\ \boldsymbol{\eta}[n] &\triangleq [\eta_1[n] \ \eta_2[n] \ \cdots \ \eta_{N_r}[n]]^T, \end{aligned}$$

as the spatial receive signal vector, transmit signal vector and the channel noise vector, respectively, then (2.2) can be written as

$$\mathbf{x}[n] = \sum_{\ell} \mathbf{H}_{\ell} \mathbf{u}[n - \ell] + \boldsymbol{\eta}[n], \quad (2.3)$$

where $[\mathbf{H}_\ell]_{k,i} = h_{k,i}[\ell]$ is the $N_r \times N_t$ channel matrix of order q , that is,

$$\mathbf{H}(z) = \sum_{\ell=0}^q \mathbf{H}_\ell z^{-\ell}$$

is the channel transfer function matrix.

Assuming L OFDM symbols are transmitted. Defining the convolution matrix

$$\mathbf{H} \triangleq \begin{bmatrix} \mathbf{H}_0 & \mathbf{H}_1 & \cdots & \mathbf{H}_q & \mathbf{0} & \cdots & \cdots & \mathbf{0} \\ \mathbf{0} & \mathbf{H}_0 & \mathbf{H}_1 & \cdots & \mathbf{H}_q & \mathbf{0} & \cdots & \mathbf{0} \\ \vdots & \ddots & \ddots & \ddots & \ddots & \ddots & \ddots & \vdots \\ \mathbf{0} & \cdots & \cdots & \mathbf{0} & \mathbf{H}_0 & \mathbf{H}_1 & \cdots & \mathbf{H}_q \end{bmatrix},$$

and

$$\begin{aligned} \check{\mathbf{x}}[n] &\triangleq [\mathbf{x}^T[n] \quad \mathbf{x}^T[n-1] \quad \cdots \quad \mathbf{x}^T[n-L+1]]^T, \\ \check{\mathbf{u}}[n] &\triangleq [\mathbf{u}^T[n] \quad \mathbf{u}^T[n-1] \quad \cdots \quad \mathbf{u}^T[n-L-q+1]]^T, \\ \check{\boldsymbol{\eta}}[n] &\triangleq [\boldsymbol{\eta}^T[n] \quad \boldsymbol{\eta}^T[n-1] \quad \cdots \quad \boldsymbol{\eta}^T[n-L+1]]^T \end{aligned}$$

as the spatiotemporal received signal vector, transmitted signal vector and noise vector, respectively, then (2.3) can be expressed as

$$\check{\mathbf{x}}[n] = \mathbf{H}\check{\mathbf{u}}[n] + \check{\boldsymbol{\eta}}[n].$$

2.3 Frame Format

Conventionally, information in the physical layer is divided into frames for transmission, where each frame consists of a header followed by a payload. The header contains the preambles, which is a unique identifier that can be used for synchronization and channel estimation. The payload contains both actual data along with intermittent pilot symbols that are used to establish and maintain CSI during transmission. However, assuming there is no amplitude, phase and permutation ambiguity, the pilot symbols are not needed for the blind equalization system under consideration because equalization can be achieved by only utilizing the portion of the payload. Synchronization can also be achieved by a number of techniques such as [28], [29] and [30], and it is not considered in this thesis. The frame format contains 400 OFDM symbols with CP inserted between OFDM symbols.

Table 2.1 shows a summary of frame format.

Table 2.1: Summary of frame format

IFFT/FFT block size	64
Number of OFDM symbol in one frame	400
Number of data subcarriers	64
Number of pilot subcarriers	0
Length of cyclic prefix	$\frac{1}{4}$ OFDM symbol length
Constellation mapper	QPSK
Coded bits per subcarrier	2

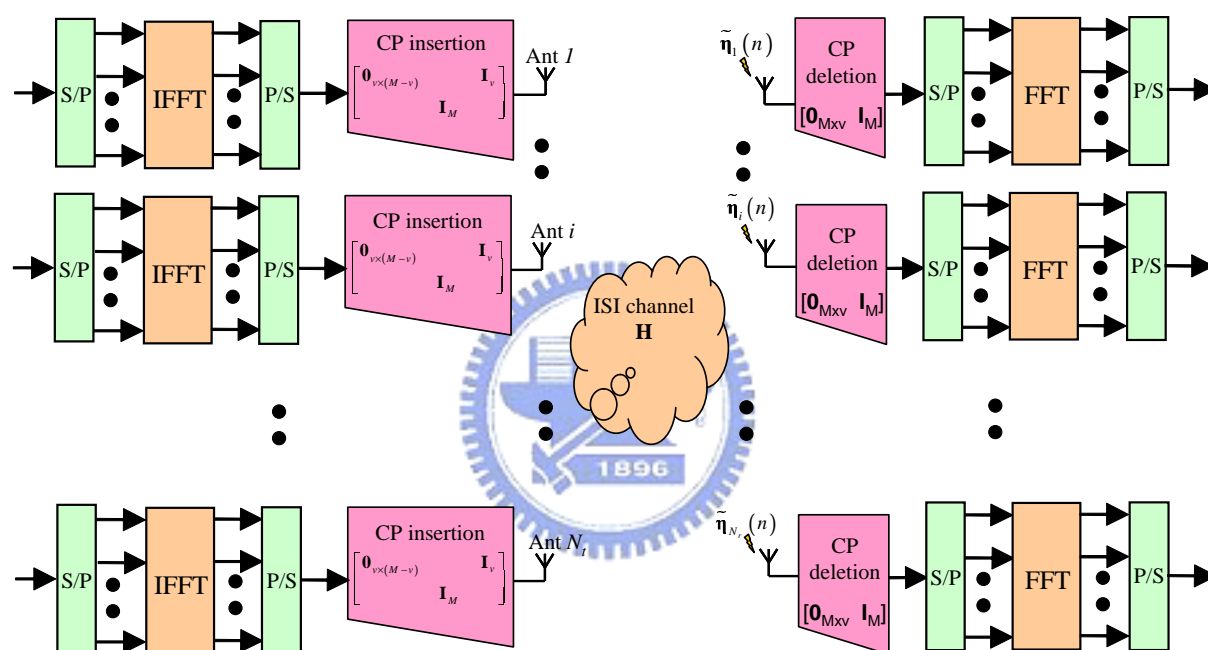


Figure 2.8: MIMO-OFDM system

Chapter 3

Precoder-Blind Equalization

Algorithm for MIMO-OFDM

3.1 SOS-Based Blind Identifiability and Equalizability Conditions for FIR-MIMO Systems

3.1.1 Identifiability Conditions

In this section, we will review the necessary and sufficient conditions for SOS-based blind identifiability as stated in [18]. Denoting the power spectral density matrix of $\mathbf{u}[n]$ as $\mathbf{S}_{\mathbf{uu}}(z)$ and let $\mathbf{H}(z)$ be the z -transform of the channel matrix \mathbf{H}_ℓ as defined in Section 2.2.2. A FIR-MIMO system is blindly identifiable up to a permutation and scaling if (a) $\mathbf{H}(z)$ is (column) irreducible and (b) $\mathbf{S}_{\mathbf{uu}}(z)$ is diagonal with distinct diagonal (rational or polynomial) functions. A polynomial matrix $\mathbf{H}(z)$ is said to be irreducible if the greatest common divisor of its $N_t \times N_t$ minors is 1. In other words, $\mathbf{H}(z)$ has full column rank for almost all z except for $z = 0$. Two polynomial or rational functions are defined to be distinct if they differ from each other by more than one constant factor, and therefore different sets of zeros and poles are required by (b). Condition (b) implies that the input

signals are spatially uncorrelated from each other but temporally correlated with distinct power spectrums. However, methods to make transmitted signal satisfying condition (b) are not discussed in [18]. In this thesis, a low computational complexity precoder that can satisfy condition (b) is proposed to blindly equalize $\mathbf{H}(z)$. Details of its design will be discussed in Section 3.3.

Note that the conditions discussed in [18] are less stringent than those previously proposed in [15], where $\mathbf{H}(z)$ is required to be both irreducible and column-reduced, which put harsher restrictions on the class of FIR-MIMO channels that can be blindly estimated by using SOS of the received signal.

3.1.2 Equalizability Conditions

Traditionally, work done on blind channel identification and equalization has mainly focused on the former; with the assumption that the equalizer can be designed based on channel estimates using different criteria such as zero-forcing or minimum mean-square error. However, as we have alluded before, it is often better to directly design the equalizer because this will implicitly take into account the channel estimate error. This has led a number of researchers to wonder if the identifiability conditions stated in the previous section is necessary (and perhaps sufficient) for the design of a SOS based blind equalizer that can directly equalize FIR-MIMO channels. Surprisingly, [31] has recently shown that in fact the conditions for direct equalizability is much weaker than those of identifiability. In this section, we shall elaborate what these conditions are and discuss the similarities between our proposed design with that of [31].

In [31], it stated that if there exists a FIR filter with transfer function, $\mathbf{W}(z)$, such that

$$\mathbf{W}(z)\mathbf{H}(z) = \mathbf{P}\mathbf{D}\mathbf{\Lambda}(z),$$

where \mathbf{P} is a permutation matrix, \mathbf{D} is a regular constant diagonal matrix, and $\mathbf{\Lambda}(z)$ is a

$N \times N$ regular diagonal matrix with diagonal entries being monic monomials, then $\mathbf{H}(z)$ is defined as equalizable. Based on this definition, it was proven in [31] that if $\mathbf{H}(z)$ is equalizable, then $\mathbf{H}(z)$ can be uniquely factorized (up to multiplication with a unitary matrix) as

$$\mathbf{H}(z) = \mathbf{H}_I(z)\mathbf{H}_P(z), \quad (3.1)$$

where $\mathbf{H}_I(z)$ is a $N_r \times N_t$ irreducible matrix with $\deg(\mathbf{H}_I(z)) \leq \deg(\mathbf{H}(z))$ and $\mathbf{H}_P(z)$ is a $N_t \times N_t$ paraunitary matrix. We will show that (3.1) is consistent with the overall system response of the proposed precoder-blind equalizer system in Section 3.2.2. Hence, unlike the identifiability conditions previously stated in the last section, the equalizability conditions do not require $\mathbf{H}(z)$ to be irreducible and column-reduced. This allows a larger class of channels which cannot be previously identified blindly by SOS based techniques, but can now be directly equalized blindly by SOS based methods. It was also shown in [32] that using SOS of the received signal is insufficient to equalize $\mathbf{H}(z)$ unless the transmitted signal is temporally colored. Such condition coincides with the identifiability conditions stated in [18], which motivates the development of our proposed precoder-blind equalizer algorithm.

3.2 SOS-Based Blind Channel Identification and Equalization

3.2.1 Existing SOS-Based Periodic Precoding Channel Identification

An existing SOS based blind channel identification scheme for MIMO-OFDM systems [21] is reviewed in this section, which will be compared with the presented algorithm in Section 3.4. Although the scheme proposed in [21] is a two-step equalizer system instead of

direct equalization, it exploits precoding and SOS of received signal to estimate channel. Therefore, we choose this algorithm as comparison with the proposed one. The basic idea of [21] is to exploit periodic nonconstant-modulus precoding at the transmitter such that a separate identification of the individual scalar subchannels $h_{i,j}[\ell]$ can be achieved by cyclostationary statistics. Providing each transmit antenna with a different signature in the cyclostationary domain, the cyclic power spectrum matrices of all transmit antennas except one will be zero for a given cycle. Thereby, it is possible to identify the entire channel system on a column by column basis (subchannel by subchannel basis) up to a constant diagonal matrix of phase rotations.

The inherent ambiguity can be resolved using short training sequences in practice, and hence we usually assume that the ambiguity is known or solved. Altogether, periodic precoding serves to transform the whole MIMO channel identification into several scalar subchannel problems, and the redundancy introduced by the CP is used to blindly identify these scalar subchannels.

At the transmitter, the individual data streams are multiplied by P -periodic precoding sequences prior to transmission. The precoding sequences are required to be different for different transmit antennas. Using the notation in Section 2.2.2, the precoded transmitted signal of the i^{th} transmit antenna can be written by

$$u_i[n] = \sum_{\ell} a_{\ell}^{(i)} g[n - \ell K] \sum_{m=0}^{M-1} s_{m,\ell}^{(i)} e^{j\frac{2\pi}{M}m(n-\ell K)},$$

$$i = 1, 2, \dots, N_t,$$

where $a_{\ell}^{(i)}$ and $s_{m,\ell}^{(i)}$ denote the precoding sequence and data symbol on the m^{th} tone of the ℓ^{th} OFDM symbol from the i^{th} antenna, respectively. Noting that $a_{\ell}^{(i)} = a_{\ell+P}^{(i)}$, which is P -periodic. The entire ℓ^{th} OFDM symbol transmitted from the i^{th} antenna are multiplied by $a_{\ell}^{(i)}$ before IFFT is applied. Since $a_{\ell}^{(i)}$ is constant over the entire OFDM symbol, this multiplication can also be performed equivalently in the time-domain after the IFFT and parallel-to-serial conversion. Defining a $N_r \times N_r$ cyclic correlation matrix of the receive

signal vector $\mathbf{x}[n]$ as

$$\mathbf{R}_{\mathbf{xx}}[n, \tau] = E [\mathbf{x}[n]\mathbf{x}^H[n - \tau]].$$

Assuming that channel noise is statistically independent of the source data $s_{m,\ell}^{(i)}$, it was shown in [21] that

$$\mathbf{R}_{\mathbf{xx}}[n, \tau] = \sum_{\ell} \mathbf{H}_{\ell} \sum_r \mathbf{R}_{\mathbf{uu}}[n - \ell, r] \mathbf{H}_{r-\tau+\ell}^H + \mathbf{R}_{\boldsymbol{\eta}\boldsymbol{\eta}}[\tau], \quad (3.2)$$

where

$$\begin{aligned} \mathbf{R}_{\boldsymbol{\eta}\boldsymbol{\eta}}[\tau] &= E [\boldsymbol{\eta}[n]\boldsymbol{\eta}^H[n - \tau]], \\ \mathbf{R}_{\mathbf{uu}}[n, \tau] &= E [\mathbf{u}[n]\mathbf{u}^H[n - \tau]] \\ &= \text{diag}\{r_{uu}^{(i)}[n, \tau]\}_{i=1}^{N_t}. \end{aligned}$$

Since the precoding sequences $a_{\ell}^{(i)}$ is P -periodic, it can be shown that

$$\mathbf{R}_{\mathbf{uu}}[n, \tau] = \mathbf{R}_{\mathbf{uu}}[n + PK, \tau], \quad (3.3)$$

which shows that $\mathbf{u}[n]$ is a PK -periodic cyclostationary transmit signal vector. That is, each of the entries in $\mathbf{u}[n]$ is a scalar cyclostationary random process with cyclostationarity period PK . From (3.2) and (3.3), it can be shown that $\mathbf{R}_{\mathbf{xx}}[n, \tau] = \mathbf{R}_{\mathbf{xx}}[n + PK, \tau]$ such that $\mathbf{x}[n]$ is a cyclostationary receive signal vector with period PK as well.

Due to the PK -periodicity of $\mathbf{R}_{\mathbf{xx}}[n, \tau]$ in n , the Fourier series coefficients with respect to n can be expanded from $\mathbf{R}_{\mathbf{xx}}[n, \tau]$. The Fourier series coefficient matrices can be written as

$$\begin{aligned} \tilde{\mathbf{R}}_{\mathbf{xx}}[k, \tau] &= \frac{1}{PK} \sum_{n=0}^{PK-1} \mathbf{R}_{\mathbf{xx}}[n, \tau] e^{-j\frac{2\pi}{PK}kn}, \\ k &= 0, 1, \dots, PK - 1. \end{aligned}$$

The cyclic power spectral matrices can then be obtained by the use of z -transform with respect to τ , which is given by

$$\begin{aligned} \mathbf{S}_{\mathbf{xx}}[k, z] &= \sum_{\tau} \tilde{\mathbf{R}}_{\mathbf{xx}}[k, \tau] z^{-\tau} \\ &= \mathbf{H}(ze^{j\frac{2\pi}{PK}k}) \mathbf{S}_{\mathbf{uu}}[k, z] \mathbf{H}^H(1/z^*) + \mathbf{S}_{\boldsymbol{\eta}\boldsymbol{\eta}}(z) \delta[k], \end{aligned} \quad (3.4)$$

where

$$\begin{aligned}
\mathbf{S}_{\eta\eta}(z) &= \sum_{\tau} \mathbf{R}_{\eta\eta}[\tau] z^{-\tau}, \\
\mathbf{S}_{\mathbf{u}\mathbf{u}}[k, z] &= \text{diag}\{S_{uu}^{(i)}[k, z]\}_{i=1}^{N_t} \\
&= \sum_{\tau} \tilde{\mathbf{R}}_{\mathbf{x}\mathbf{x}}[k, \tau] z^{-\tau} \\
&= \sum_{\tau} \frac{1}{PK} \sum_{n=0}^{PK-1} \mathbf{R}_{\mathbf{u}\mathbf{u}}[n, \tau] e^{-j\frac{2\pi}{PK}kn} z^{-\tau}.
\end{aligned}$$

An example consisting a 2×2 MIMO-OFDM system with $P = 4$ was given in [21] to illustrate the effectiveness of the algorithm. From (3.4), it can be shown that

$$\begin{aligned}
[\mathbf{S}_{\mathbf{x}\mathbf{x}}[k, z]]_{0,0} &= H_{0,0}(ze^{j\frac{2\pi}{PK}k})S_{uu}^{(0)}[k, z]H_{0,0}^*(1/z^*) \\
&+ H_{0,1}(ze^{j\frac{2\pi}{PK}k})S_{uu}^{(1)}[k, z]H_{0,1}^*(1/z^*),
\end{aligned} \tag{3.5}$$

and

$$\begin{aligned}
[\mathbf{S}_{\mathbf{x}\mathbf{x}}[k, z]]_{1,1} &= H_{1,0}(ze^{j\frac{2\pi}{PK}k})S_{uu}^{(0)}[k, z]H_{1,0}^*(1/z^*) \\
&+ H_{1,1}(ze^{j\frac{2\pi}{PK}k})S_{uu}^{(1)}[k, z]H_{1,1}^*(1/z^*).
\end{aligned} \tag{3.6}$$

To separating the subchannels, the goal is to find cycles $k_1 \neq 0$ and $k_2 \neq 0$, which satisfy

$$\begin{aligned}
S_{uu}^{(0)}[k_1, z] &= 0, S_{uu}^{(1)}[k_1, z] \neq 0, \\
S_{uu}^{(1)}[k_2, z] &= 0, S_{uu}^{(0)}[k_2, z] \neq 0.
\end{aligned}$$

In [21], it was shown that the Fourier series coefficient matrix $\tilde{\mathbf{R}}_{\mathbf{u}\mathbf{u}}[k, \tau]$ can be written as

$$\begin{aligned}
\tilde{\mathbf{R}}_{\mathbf{u}\mathbf{u}}[k, \tau] &= \text{diag}\{\tilde{R}_{uu}^{(i)}[k, \tau]\}_{i=1}^{N_t} \\
&= \frac{M}{PK} \delta_M[\tau] A^{(g,g)} \left[\tau, \frac{k}{PK} \right] \times \text{diag} \left\{ \sigma_i^2 \Phi_P^{(i)}[k] \right\}_{i=1}^{N_t},
\end{aligned} \tag{3.7}$$

where

$$\begin{aligned}\Phi_P^{(i)}[k] &= \sum_{r=0}^{P-1} |a_r^{(i)}|^2 e^{-j\frac{2\pi}{P}rk}, \\ A^{(g,g)}\left[\tau, \frac{k}{PK}\right] &= \frac{1}{M} e^{-j2\pi\frac{k}{PK}\frac{K+\tau-1}{2}} \\ &\quad \times \begin{cases} \frac{\sin(\frac{\pi k}{PK}(K-\tau))}{\sin(\pi\frac{k}{PK})}, & 0 \leq \tau \leq K-1 \\ \frac{\sin(\frac{\pi k}{PK}(K+\tau))}{\sin(\pi\frac{k}{PK})}, & -K+1 \leq \tau < 0. \end{cases}\end{aligned}$$

Since $S_{ss}^{(i)}[k, z] = \sum_{\tau} \tilde{R}_{ss}^{(i)}[k, \tau] z^{-\tau}$, we have $S_{ss}^{(i)}[k, z] = 0$ if and only if $\tilde{R}_{ss}^{(i)}[k, \tau] = 0$.

Therefore, the solution for k can be found by choosing k_1 and k_2 such that

$$\begin{aligned}\Phi_P^{(0)}[k_1] &= 0, \Phi_P^{(1)}[k_1] \neq 0, \\ \Phi_P^{(1)}[k_2] &= 0, \Phi_P^{(0)}[k_2] \neq 0.\end{aligned}$$

Setting k to be k_1 and k_2 in $[\mathbf{S}_x[k, z]]_{0,0}$ and $[\mathbf{S}_x[k, z]]_{1,1}$ and noting that $\Phi_P^{(i)}[-k] = \Phi_P^{(i)*}[k]$, from (3.5) and (3.6) it follows that

$$[\mathbf{S}_{xx}[\pm k_1, z]]_{0,0} = H_{0,1} \left(z e^{\pm j\frac{2\pi}{PK}k_1} \right) S_{uu}^{(1)}[\pm k_1, z] H_{0,1}^*(1/z^*), \quad (3.8)$$

$$[\mathbf{S}_{xx}[\pm k_1, z]]_{1,1} = H_{1,1} \left(z e^{\pm j\frac{2\pi}{PK}k_1} \right) S_{uu}^{(1)}[\pm k_1, z] H_{1,1}^*(1/z^*), \quad (3.9)$$

$$[\mathbf{S}_{xx}[\pm k_2, z]]_{0,0} = H_{0,0} \left(z e^{\pm j\frac{2\pi}{PK}k_2} \right) S_{uu}^{(0)}[\pm k_2, z] H_{0,0}^*(1/z^*), \quad (3.10)$$

$$[\mathbf{S}_{xx}[\pm k_2, z]]_{1,1} = H_{1,0} \left(z e^{\pm j\frac{2\pi}{PK}k_2} \right) S_{uu}^{(0)}[\pm k_2, z] H_{1,0}^*(1/z^*). \quad (3.11)$$

It is clear that the subchannels $H_{0,1}(z)$ and $H_{1,1}(z)$ can be identified from (3.8) and (3.9), respectively. Similarly, the subchannels $H_{0,0}(z)$ and $H_{1,0}(z)$ can be identified from (3.10) and (3.11), respectively. As a result, the 2×2 MIMO channel identification problem is transformed into a identification problem of four scalar subchannels.

The algorithm previously proposed in [33] and [34] can be exploited to identify the individual scalar subchannels. The following discussion is restricted to the identification of $H_{0,0}(z)$ only because the remaining subchannels can be identified using the same

procedure. Starting from (3.10), it can be shown that

$$[\mathbf{S}_{\mathbf{xx}}[k_2, z)]_{0,0} S_{uu}^{(0)}[-k_2, z] H_{0,0}(ze^{-j\frac{2\pi}{PK}k_2}) - [\mathbf{S}_{\mathbf{xx}}[-k_2, z)]_{0,0} S_{uu}^{(0)}[k_2, z] H_{0,0}(ze^{j\frac{2\pi}{PK}k_2}) = 0. \quad (3.12)$$

From (3.12), straightforward manipulations show that

$$\sum_{\ell=0}^{L_{h_{0,0}}-1} [a_{x,u}^{(k_2, -k_2)}[n - \ell] e^{j\frac{2\pi}{PK}k_2\ell} - a_{x,u}^{(-k_2, k_2)}[n - \ell] e^{-j\frac{2\pi}{PK}k_2\ell}] h_{0,0}[\ell] = 0, \quad (3.13)$$

where

$$a_{x,u}^{(k,\ell)}[n] = \sum_j [\tilde{\mathbf{R}}_{\mathbf{xx}}[k, j]]_{(0,0)} C_u^{(0)}[\ell, n - j] \quad (3.14)$$

and $L_{h_{0,0}}$ is the length of the impulse response of the subchannel $H_{0,0}(z)$. Because OFDM-based systems require an upper bound on channel order to correctly choose the CP length, a safe estimate of $L_{h_{0,0}}$ can be assumed to be available and known. From (3.7), we can then obtain that $\tilde{R}_{uu}^{(0)}[k, \tau] \neq 0$ for $\tau = -M, 0, M$, and $\tilde{R}_{uu}^{(0)}[k, \tau] = 0$ else. This implies that

$$\begin{aligned} a_{x,u}^{(k,\ell)}[n] &= [\tilde{\mathbf{R}}_{\mathbf{xx}}[k, n]]_{0,0} R_{uu}^{(0)}[\ell, 0] \\ &+ [\tilde{\mathbf{R}}_{\mathbf{xx}}[k, n - M]]_{0,0} R_{uu}^{(0)}[\ell, M] \\ &+ [\tilde{\mathbf{R}}_{\mathbf{xx}}[k, n + M]]_{0,0} R_{uu}^{(0)}[\ell, -M]. \end{aligned}$$

For the purpose of solving the subchannel $H_{0,0}$, (3.13) is rewritten for convenience in vector-matrix form as

$$[\mathbf{T}_{x,u}^{(k_2, -k_2)} \mathbf{D}^{-k_2} - \mathbf{T}_{x,u}^{(-k_2, k_2)} \mathbf{D}^{k_2}] \mathbf{h}_{0,0} = \mathbf{0}, \quad (3.15)$$

where $\mathbf{T}_{x,u}^{(k,\ell)}$ is a the $(4K + 3L_{h_{0,0}} - 6) \times L_{h_{0,0}}$ Toeplitz matrix with the first row equal to

$$[a_{x,u}^{(k,\ell)}[-2K - L_{h_{0,0}} + 3] \quad 0 \quad \dots \quad 0]$$

and the first column equal to

$$[a_{x,u}^{(k,\ell)}[-2K - L_{h_{0,0}} + 3] \quad \dots \quad a_{x,u}^{(k,\ell)}[2K + L_{h_{0,0}} - 3] \quad 0 \quad \dots \quad 0]^T.$$

Moreover,

$$\begin{aligned} \mathbf{D} &= \text{diag}\{e^{-j\frac{2\pi}{PK}\ell}\}_{\ell=0}^{L_{h_{0,0}}-1}, \\ \mathbf{h}_{0,0} &= [h_{0,0}[0] \quad h_{0,0}[1] \quad \dots \quad h_{0,0}[L_{h_{0,0}} - 1]]^T \end{aligned}$$

and $\mathbf{0}$ represents a $4K + 3L_{h_{0,0}} - 6 \times 1$ all-zero vector. The subchannel estimate $\hat{\mathbf{h}}_{0,0}$ can then be found by solving the optimization problem given as

$$\hat{\mathbf{h}}_{0,0} = \arg \min_{\|\mathbf{h}_{0,0}\|=1} \left\| [\mathbf{T}_{x,u}^{(k_2,-k_2)} \mathbf{D}^{-k_2} - \mathbf{T}_{x,u}^{(-k_2,k_2)} \mathbf{D}^{k_2}] \mathbf{h}_{0,0} \right\|^2. \quad (3.16)$$

The other subchannels $H_{0,1}(z)$, $H_{1,1}(z)$ and $H_{1,0}$ can be estimated using the same procedure as given by (3.8), (3.9), (3.11), respectively.

In fact, an estimation of the cyclostationary statistics $\tilde{\mathbf{R}}_{\mathbf{xx}}[k, \tau]$ is exploited to replace the ideal one, which is written as

$$\hat{\tilde{\mathbf{R}}}_{\mathbf{xx}}[k, \tau] = \frac{1}{T} \sum_{n=0}^{T-1} \mathbf{x}[n] \mathbf{x}^H[n - \tau] e^{-j\frac{2\pi}{PK}kn}. \quad (3.17)$$

The estimation of $a_{x,s}^{(k,\ell)}[n]$, denoted by $\hat{a}_{x,s}^{(k,\ell)}[n]$, can then be obtained using (3.14) where $\tilde{\mathbf{R}}_{\mathbf{xx}}[k, \tau]$ is replaced by $\hat{\tilde{\mathbf{R}}}_{\mathbf{xx}}[k, \tau]$.

3.2.2 SOS-Based Precoder-Blind Equalization

To satisfy the blind identification conditions stated in Section 3.1, the transmitted signal vector $\check{\mathbf{u}}[n]$ is assumed to be spatially uncorrelated but temporally correlated with distinct power. The notation used here is the same as that in Section 2.2.2. Without loss of generality, $\check{\mathbf{u}}[n]$ can assume to have unit variance and zero mean. Define the correlation matrix of $\check{\mathbf{u}}[n]$ as $\mathbf{R}_{\check{\mathbf{u}}\check{\mathbf{u}}}[\tau] \triangleq E[\check{\mathbf{u}}[n] \check{\mathbf{u}}^H[n + \tau]]$, then $\mathbf{R}_{\check{\mathbf{u}}\check{\mathbf{u}}}[0] = \mathbf{I}_{N_t L}$. The autocorrelation matrix of $\check{\mathbf{u}}[n]$ can be expressed as

$$\begin{aligned} \mathbf{R}_{\check{\mathbf{u}}\check{\mathbf{u}}}[\tau] &= E[\check{\mathbf{u}}[n] \check{\mathbf{u}}^H[n + \tau]] \\ &= \begin{cases} \mathbf{I}_{N_t L}, & \text{for } \tau = 0, \\ \text{diag}(\rho_1[\tau], \dots, \rho_{N_t L}[\tau]), & \text{for } \tau \neq 0, \end{cases} \end{aligned}$$

where $\rho_1[\tau] \neq \dots \neq \rho_{N_t L}[\tau] \neq 0$. It is worth to note that distinct values for the diagonal elements of $\mathbf{R}_{\check{\mathbf{u}}\check{\mathbf{u}}}[\tau]$ also satisfy conditions stated in Section 3.1.2, which makes the correlation functions of all transmitted streams linearly independent. In this case, direct blind equalization can be achieved by the use of temporal SOS [31]. We further assume that $\check{\boldsymbol{\eta}}[n]$ is white Gaussian distributed and is mutually uncorrelated with $\check{\mathbf{u}}[n]$. Then the autocorrelation matrix of the channel output $\check{\mathbf{x}}[n]$ can be written as

$$\mathbf{R}_{\check{\mathbf{x}}\check{\mathbf{x}}}[\tau] = \begin{cases} \mathbf{H}\mathbf{R}_{\check{\mathbf{u}}\check{\mathbf{u}}}[0]\mathbf{H}^H + \sigma_{\check{\boldsymbol{\eta}}}^2 \mathbf{I}_{N_r(L+q)}, & \text{for } \tau = 0, \\ \mathbf{H}\mathbf{R}_{\check{\mathbf{u}}\check{\mathbf{u}}}[\tau]\mathbf{H}^H, & \text{for } \tau \neq 0, \end{cases} \quad (3.18)$$

where $\sigma_{\check{\boldsymbol{\eta}}}^2$ is the variance of the noise signal $\check{\boldsymbol{\eta}}[n]$. Defining $\check{\mathbf{v}}[n] = \mathbf{H}\check{\mathbf{u}}[n]$ as the channel output vector ignoring channel noise and

$$\mathbf{R}_{\check{\mathbf{v}}\check{\mathbf{v}}}[\tau] \triangleq E [\check{\mathbf{v}}[n]\check{\mathbf{v}}[n+\tau]^H].$$

Since $\mathbf{R}_{\check{\mathbf{u}}\check{\mathbf{u}}}[0] = \mathbf{I}_{N_t L}$, therefore

$$\mathbf{R}_{\check{\mathbf{v}}\check{\mathbf{v}}}[0] = \mathbf{H}\mathbf{H}^H.$$

Let \mathbf{W} be a whitening matrix that whitens $\check{\mathbf{v}}[n]$ such that

$$E [\mathbf{W}\check{\mathbf{v}}[n]\check{\mathbf{v}}^H[n]\mathbf{W}^H] = \mathbf{I}_{N_r(L+q)},$$

where

$$\mathbf{W} = \boldsymbol{\Sigma}_{\check{\mathbf{v}}}^{-\frac{1}{2}} \mathbf{Q}_{\check{\mathbf{v}}}^H$$

with $\boldsymbol{\Sigma}_{\check{\mathbf{v}}}^{-\frac{1}{2}}$ being the square root inverse of the eigenvalue matrix of $\mathbf{R}_{\check{\mathbf{v}}\check{\mathbf{v}}}[0]$, and $\mathbf{Q}_{\check{\mathbf{v}}}$ being the eigenvector matrix of $\mathbf{R}_{\check{\mathbf{v}}\check{\mathbf{v}}}[0]$. Then we can obtain

$$\begin{aligned} \mathbf{W}\mathbf{R}_{\check{\mathbf{v}}\check{\mathbf{v}}}[0]\mathbf{W}^H &= E [\mathbf{W}\check{\mathbf{v}}[n]\check{\mathbf{v}}^H[n]\mathbf{W}^H] \\ &= \mathbf{W}\mathbf{H}\mathbf{H}^H\mathbf{W}^H \\ &= \mathbf{I}_{N_r(L+q)}. \end{aligned} \quad (3.19)$$

According to (3.19), the effective channel $\mathbf{U} = \mathbf{W}\mathbf{H}$ is a unitary matrix such that $\mathbf{U}^H\mathbf{U} = \mathbf{U}\mathbf{U}^H = \mathbf{I}$.

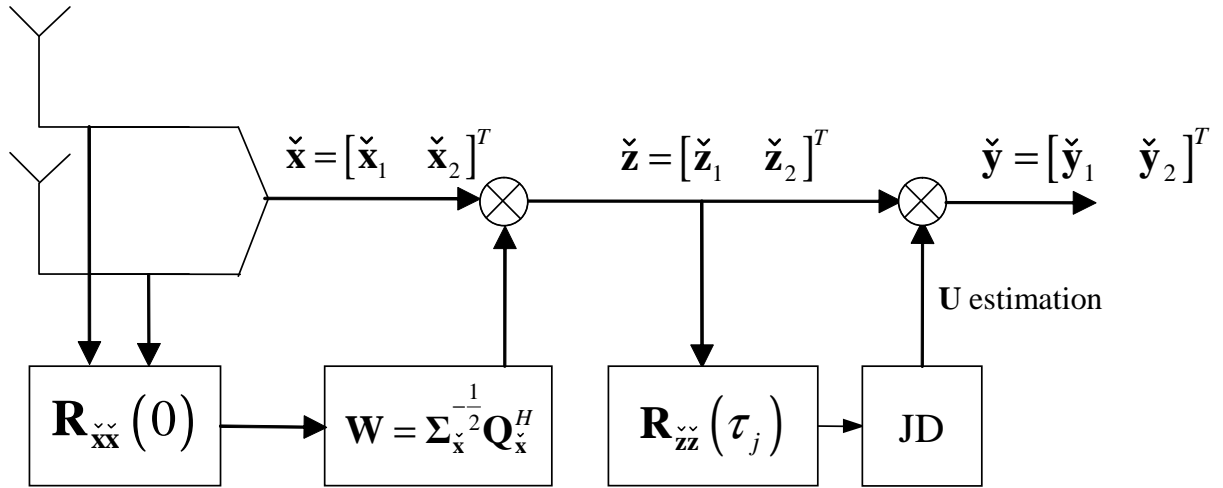


Figure 3.1: Block diagram of equalization process with 2 receive antennas where JD represents joint diagonalization.

Applying \mathbf{W} to the received signal vector $\check{\mathbf{x}}[n]$, we can obtain

$$\begin{aligned}
 \check{\mathbf{z}}[n] &= \mathbf{W}\check{\mathbf{x}}[n] \\
 &= \mathbf{W}[\mathbf{H}\check{\mathbf{u}}[n] + \check{\boldsymbol{\eta}}[n]] \\
 &= \mathbf{U}\check{\mathbf{u}}[n] + \mathbf{W}\check{\boldsymbol{\eta}}[n].
 \end{aligned} \tag{3.20}$$

From (3.20), we see that \mathbf{U} can be equalized by

$$\mathbf{U}^{-1}\check{\mathbf{z}}[n] = \mathbf{U}^H\check{\mathbf{z}}[n] = \check{\mathbf{u}}[n] + \mathbf{U}^H\mathbf{W}\check{\boldsymbol{\eta}}[n]. \tag{3.21}$$

From (3.21), the problem of equalization becomes finding the unitary equalization matrix of \mathbf{U} . Noting that $\mathbf{U}^{-1} = \mathbf{U}^H$, so the inversion of equalization matrix causing high computational complexity can be replaced by Hermitian operation. Furthermore, \mathbf{U} is consistent with the factorization (3.1) of equalizable channels stated in Section 3.1.2 because any unitary matrix is a paraunitary matrix. This implies that \mathbf{U} is equalizable. Defining the correlation matrices for $\check{\mathbf{z}}[n]$ and $\check{\boldsymbol{\eta}}[n]$ as $E[\check{\mathbf{z}}[n]\check{\mathbf{z}}^H[n+\tau]]$ and $E[\check{\boldsymbol{\eta}}[n]\check{\boldsymbol{\eta}}^H[n+\tau]]$, respectively. From (3.18), $E[\check{\boldsymbol{\eta}}[n]\check{\boldsymbol{\eta}}^H[n+\tau]] = 0$, for $\tau \neq 0$. Thus, the correlation matrix of

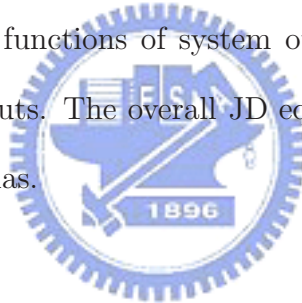
$\check{\mathbf{z}}[n]$ can be written as

$$\mathbf{R}_{\check{\mathbf{z}}\check{\mathbf{z}}}[\tau] = \mathbf{U}\mathbf{R}_{\check{\mathbf{u}}\check{\mathbf{u}}}[\tau]\mathbf{U}^H, \quad \text{for } \tau \neq 0. \quad (3.22)$$

Hence, the equalizer \mathbf{U} can be obtained by diagonalizing $\mathbf{R}_{\check{\mathbf{z}}\check{\mathbf{z}}}[\tau]$. According to [22], we can find \mathbf{U} that equalizes frequency-selective channels if the source signal has different spectral energy. In addition, the chance of eigenvalue degeneracy can also be reduced by performing a joint diagonalization on a set of $\mathbf{R}_{\check{\mathbf{z}}\check{\mathbf{z}}}[\tau]$ with various $\tau \neq 0$, i.e.

$$\mathbf{U}^H \mathbf{R}_{\check{\mathbf{z}}\check{\mathbf{z}}}[\tau_j] \mathbf{U} = \text{diag}(\rho_1[\tau_p], \rho_2[\tau_p], \dots, \rho_{N_t L}[\tau_p]), \quad \text{for } p = 0 \leq t \leq P,$$

where $\tau_0, \tau_1, \dots, \tau_P$ are non-zero time lags. Denoting the estimate of \mathbf{U} as $\hat{\mathbf{U}}$. To note that $\hat{\mathbf{U}}$ has a permutation and scalar ambiguity to \mathbf{U} . This is corresponding to the property stated in Section 3.1.2, which shows the total blind equalization system is transparent if and only if the autocorrelation functions of system outputs are the same as some permutation of those of system inputs. The overall JD equalization process is illustrated in Figure 3.1 with 2 receive antennas.



The entire equalization process is summarized as follows:

1. Estimate the autocorrelation matrix of the received signal $\mathbf{R}_{\check{\mathbf{x}}\check{\mathbf{x}}}[0]$.
2. Compute the whitening matrix \mathbf{W} by

$$\mathbf{W} = \mathbf{\Sigma}_{\check{\mathbf{x}}}^{-\frac{1}{2}} \mathbf{Q}_{\check{\mathbf{x}}}^H,$$

where $\mathbf{\Sigma}_{\check{\mathbf{x}}}$ is the eigenvalue matrix of $\mathbf{R}_{\check{\mathbf{x}}\check{\mathbf{x}}}[0]$,

and $\mathbf{Q}_{\check{\mathbf{x}}}$ is the eigenvector matrix of $\mathbf{R}_{\check{\mathbf{x}}\check{\mathbf{x}}}[0]$.

3. Whiten the received vector $\check{\mathbf{x}}[n]$ by \mathbf{W} to obtain $\check{\mathbf{z}}[n] = \mathbf{W}\check{\mathbf{x}}[n]$.
4. Obtain a set of correlation matrices $\mathbf{R}_{\check{\mathbf{z}}\check{\mathbf{z}}}[\tau_p]$ of the whitened vector $\check{\mathbf{z}}[n]$ for $p = 0, 1, \dots, P$.
5. Perform JD on the set of $\mathbf{R}_{\check{\mathbf{z}}\check{\mathbf{z}}}[\tau_p]$ for $p = 0, 1, \dots, P$ to estimate the equalization matrix \mathbf{U} .
6. Equalize $\check{\mathbf{z}}[n]$ by \mathbf{U}^H to obtain the estimate of $\check{\mathbf{u}}[n]$.
7. Remove the temporal correlation of the equalized signal by decoloring decoders after FFT.

3.3 Precoder Design

3.3.1 Precoder Format

If all the source data streams are uncorrelated, then the required temporal correlation property can be easily achieved by shaping the power spectral density of each data stream [18]. [22] proposed to use a set of low complexity precoders to color the source signal stream such that FIR blind equalization is possible at the receiver to equalize FIR-MIMO channels. However, the precoders in [22] were chosen arbitrarily without regards on its

effects on BER performance. Moreover, no investigation was carried out about how the precoder can be used to reduce computational complexity at the receiver while sustaining equalization performance. In this thesis, a new set of precoders are proposed that will allow us to select a subset of $\{\mathbf{R}_{\mathbf{z}\mathbf{z}}(\tau_p)\}$ such that it not only reduces the computational complexity at the receiver, but it also does not impact the equalization performance compare to the case when the full set of autocorrelation matrices are used. As seen in Figure 3.2, the precoders are applied in the frequency domain (prior to IFFT) to all N_t transmit antennas of a MIMO-OFDM system. Compared with [22], the precoders for OFDM-based systems can be simplified to multiplication over all subcarriers due to IFFT. The set of coloring precoders are denoted as $\{\mathbf{P}_0(z), \mathbf{P}_1(z), \dots, \mathbf{P}_{N_t-1}(z)\}$, where

$$\mathbf{P}_i(z) = \text{diag}(\alpha_{i,0}, \alpha_{i,1}, \dots, \alpha_{i,M-1}) \quad \text{for } i = 1, 2, \dots, N_t.$$

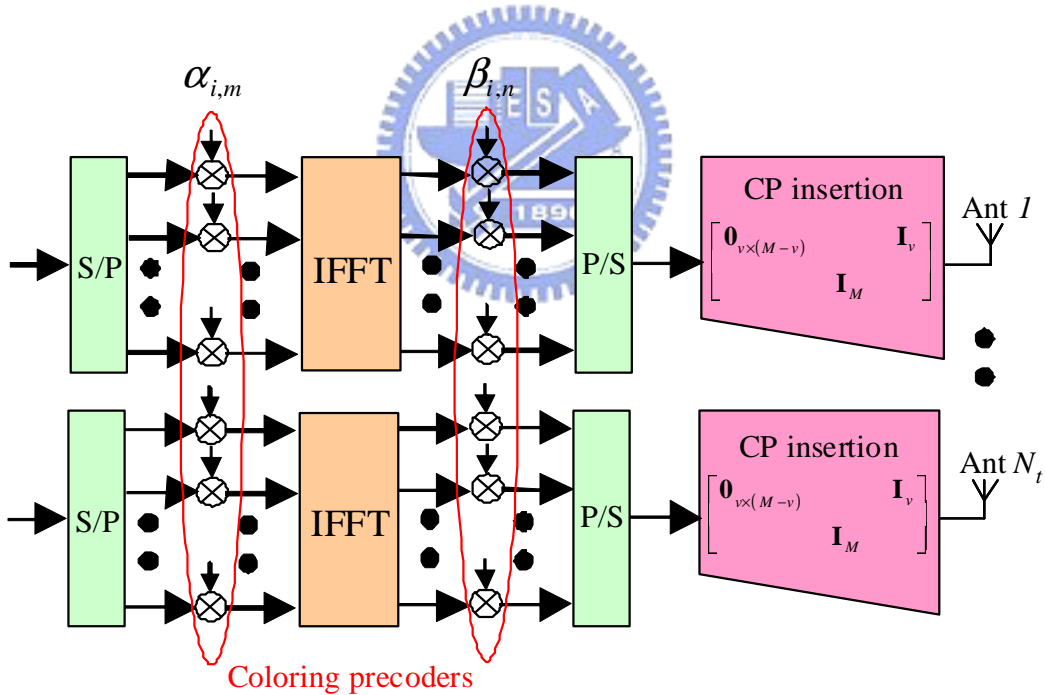


Figure 3.2: The transmitter of the precoder-blind equalizer system with 2 Tx/Rx antennas.

$\alpha_{i,m}$ is the real-valued multiplier coefficient of the m^{th} path of IFFT for the i^{th} transmit antenna as illustrated in Figure 3.2. A scaling matrix is then applied in the time domain,

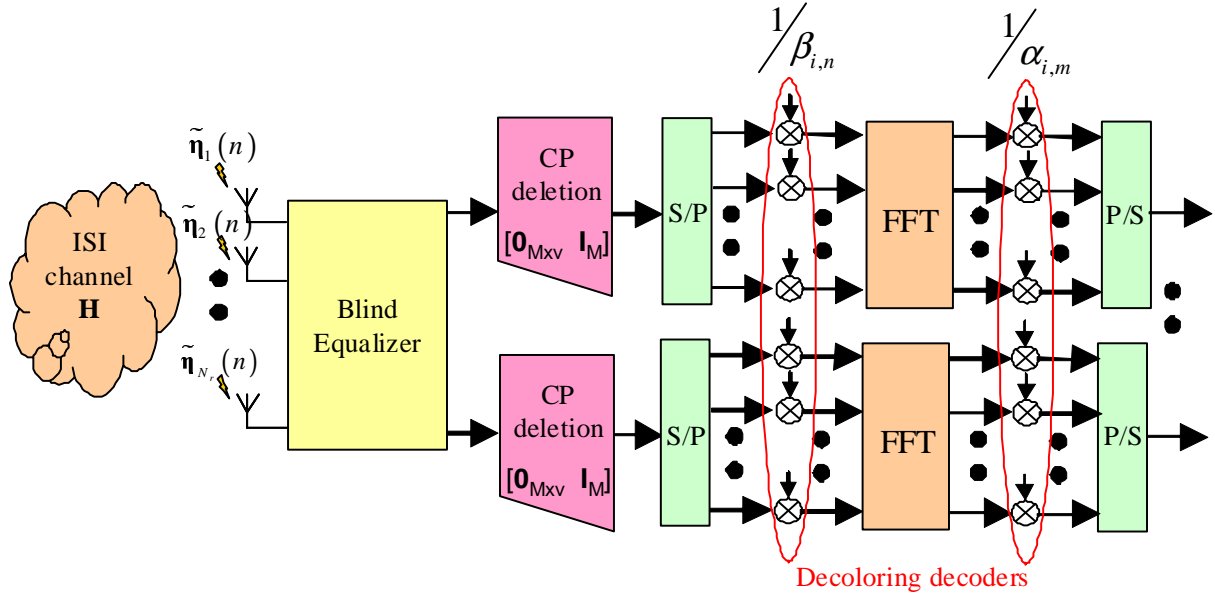


Figure 3.3: The receiver of the precoder-blind equalizer system with 2 Tx/Rx antennas.

which is given as

$$\mathbf{S}_i(z) = \text{diag}(\beta_{i,0}, \beta_{i,1}, \dots, \beta_{i,M-1}) \quad \text{for } i = 1, 2, \dots, N_t,$$

where $\beta_{i,n}$ is a scaling factor that is used to satisfy the distinct power condition. At the receiver, the multiplicative inverse of the precoders is used to decolor the colored signal as shown in Figure 3.3. The proposed real-valued multiplier $\alpha_{i,m}$ is formed with two parts. The first part generates the orthogonality among different precoders, and the second part introduces temporal correlation to the transmitted signal. Since the performance of the joint diagonalization algorithm is based on spectral overlap of the source signals [20], this led to the use of orthogonal precoders. $\alpha_{i,m}$ can be expressed as

$$\alpha_{i,m} = O_i(m) \left[1 - \sum_{p=0}^{P-1} C_{i,\tau_p} \cos\left(\frac{2\pi m \tau_p}{M}\right) \right], \quad (3.23)$$

where $O_i(m)$ is a function having only two possible values $+1$ and -1 . $O_i(m)$ can be designed to generate orthogonality among different precoders by being assigned different shape for different precoders. C_{i,τ_p} determines the magnitude of corresponding cosine term. Distinct values of C_{i,τ_p} must be used for various values of n and p in order to

satisfy the distinct power conditions in [18]. The number of cosine term can be decided arbitrarily by choosing P . Furthermore, different τ_p is used for different cosine terms with $\tau_p = 0, 1, \dots, P - 1$.

3.3.2 Temporal Correlation Injection

The reason for using cosine is because we can completely control how many autocorrelation matrices in $\{R_{\mathbf{z}\mathbf{z}}(\tau_p)\}$ we need in (3.23) for the joint diagonalization. Namely, the autocorrelation matrices needed by joint diagonalization can be determined using this form of precoders at the transmitter. Once the needed autocorrelation matrices are known, the range for the lag can be dramatically reduced. Therefore, the latency and computational complexity at the receiver are both decreased. This can be seen by considering the inverse Fourier transform of $\cos\left(\frac{2\pi m\tau_p}{M}\right)$, which is written as

$$\begin{aligned}
 \mathcal{F}^{-1}\left\{\cos\left(\frac{2\pi m\tau_p}{M}\right)\right\} &= \sum_{m=0}^{M-1} \cos\left(\frac{2\pi m\tau_p}{M}\right) e^{\frac{j2\pi mn}{M}} \\
 &= \frac{1}{2} \left[\sum_{m=0}^{M-1} e^{\frac{j2\pi m(n+\tau_p)}{M}} + \sum_{m=0}^{M-1} e^{\frac{j2\pi m(n-\tau_p)}{M}} \right] \\
 &= \frac{1}{2} (\delta[n + \tau_p] + \delta[n - \tau_p]).
 \end{aligned} \tag{3.24}$$

As a result, the output of the IFFT can be given by

$$\begin{aligned}
 \check{u}(n) & * \left\{ 1 - \frac{C_{i,\tau_0}}{2} (\delta[n + \tau_0] + \delta[n - \tau_0]) \right\} \\
 &= \check{u}(n) - \frac{C_{i,\tau_0}}{2} (\check{u}[n + \tau_0] + \check{u}[n - \tau_0]),
 \end{aligned} \tag{3.25}$$

where $*$ denotes convolution and $P = 1$. From (3.25), it is apparent that temporal correlation of lag τ_0 can be generated. The autocorrelation function of the i^{th} transmit

antenna for τ_0 can also be given as

$$\begin{aligned}
r_i[\tau_0] &= E [u_i[n]u_i[n + \tau_0]] \\
&= E \left[\left\{ \tilde{s}_i[n] - \frac{C_{i,\tau_0}}{2}(\tilde{s}_i[n + \tau_0] + \tilde{s}_i[n - \tau_0]) \right\} \left\{ \tilde{s}_i[n + \tau_0] - \frac{C_{i,\tau_0}}{2}(\tilde{s}_i[n + 2\tau_0] + \tilde{s}_i[n]) \right\} \right] \\
&= -\frac{C_{i,\tau_0}}{2} E [\tilde{s}_i^2[n] + \tilde{s}_i^2[n + \tau_0]] \\
&= -C_{i,\tau_0} E [\tilde{s}_i^2[n]] \\
&= -C_{i,\tau_0},
\end{aligned}$$

which is completely controlled by the coefficient of the cosine term. Therefore, only $\mathbf{R}_{\tilde{\mathbf{z}}\tilde{\mathbf{z}}}(\tau_0)$ will have to be used by the joint diagonalizer at the receiver. In fact, using the rest of the $\mathbf{R}_{\tilde{\mathbf{z}}\tilde{\mathbf{z}}}(\tau_p)$, $\forall p \neq 0$ will not improve the equalization performance. This will be verified in the simulation results in the next section when we compare equalization performance of our proposed algorithm using different τ_p . Besides varying τ_p , the parameter P can also be used to improve performance of the equalizer. This can be achieved by increasing the value of P such that more temporal correlation is added to the transmitted bitstream. However, as will be seen in Section 3.4, P cannot be increased indefinitely because the precoder will introduce too much amplitude variation into the bitstream which degrades the BER performance, even though a better estimation of \mathbf{U} can be obtained.

According to the blind identification conditions stated in [18] and the MIMO-OFDM system model stated in Section 2.2.2, correlation matrix $\mathbf{R}_{\mathbf{uu}}(\tau)$ must have distinct diagonal power. In other words, C_{i,τ_p} has to be assigned various values for different transmit antennas and time index n . In order to satisfy this condition, we consider a set of coefficients c_0, c_1, \dots, c_w , where $w = \max\{L + q - 1, N_t P - 1\}$, for the value of C_{i,τ_p} . Let the time index n be $n = 0, 1, \dots, L + q - 1$. Table 3.1 and 3.2 list the values for C_{i,τ_p} for different values of p and at different time. As seen in the tables, the coefficients for the current time instant are a left-shifted version of those at the previous time instant. For example, when $n = 0$, $C_{1,\tau_0} = c_0$, $C_{1,\tau_1} = c_1, \dots, C_{N_t,\tau_{P-2}} = c_{N_t P - 2}$, $C_{N_t,\tau_{P-1}} = c_{N_t P - 1}$.

Table 3.1: Values for C_{i,τ_p} for $L + q > N_t P$

n	C_{1,τ_0}	C_{1,τ_1}	\cdots	$C_{N_t,\tau_{P-2}}$	$C_{N_t,\tau_{P-1}}$
0	c_0	c_1	\cdots	$c_{N_t P - 2}$	$c_{N_t P - 1}$
1	c_1	c_2	\cdots	$c_{N_t P - 1}$	$c_{N_t P}$
2	c_2	c_3	\cdots	$c_{N_t P}$	$c_{N_t P + 1}$
\vdots	\vdots	\vdots	\cdots	\vdots	\vdots
$L + q - 1$	c_{L+q-1}	c_0	\cdots	c_{L+q-3}	c_{L+q-2}

Table 3.2: Values for C_{i,τ_p} for $L + q \leq N_t P$

n	C_{1,τ_0}	C_{1,τ_1}	\cdots	$C_{N_t,\tau_{P-2}}$	$C_{N_t,\tau_{P-1}}$
0	c_0	c_1	\cdots	$c_{N_t P - 2}$	$c_{N_t P - 1}$
1	c_1	c_2	\cdots	$c_{N_t P - 1}$	c_0
2	c_2	c_3	\cdots	c_0	c_1
\vdots	\vdots	\vdots	\cdots	\vdots	\vdots
$L + q - 1$	c_{L+q-1}	c_{L+q}	\cdots	c_{L+q-3}	c_{L+q-2}

Then for $n = 1$, $C_{1,\tau_0} = c_1$, $C_{1,\tau_1} = c_2$, \cdots , $C_{N_t,\tau_{P-2}} = c_{N_t P - 1}$, $C_{N_t,\tau_{P-1}} = c_{N_t P}$, assuming that $L + q > N_t P$. If $L + q \leq N_t P$, then $C_{N_t,\tau_{P-1}} = c_0$. In other words, the coefficients are circularly rotated left with increasing time. This is mainly done as a design convenience. The coefficients will keep rotating left with time until $n = L + q - 1$, and the sequence will then repeat for subsequent time index.

An example is illustrated in Table 3.3.2, where $q = 2$ (3-tap FIR channel), $L = 2$, $P = 2$ and $N_t = 2$. Noting that $L + q = N_t P$. $\mathbf{R}_{\mathbf{uu}}(\tau_p)$ will then have distinct diagonal power for $p = 0, 1$. The distinct power required by conditions of equalizability can therefore be satisfied because all diagonal elements of correlation matrices of transmitted signal will

Table 3.3: Values for C_{i,τ_p} when $q = 2, L = 2, P = 2, N_t = 2$

$C_{1,1}$	c_0	c_1	c_2	c_3
$C_{1,2}$	c_1	c_2	c_3	c_0
$C_{2,1}$	c_2	c_3	c_0	c_1
$C_{2,2}$	c_3	c_0	c_1	c_2
n	$4k$	$4k + 1$	$4k + 2$	$4k + 3$

* $k \in \mathbb{Z}^+$

be different. This is equivalent to assigning distinct values to $\beta_{i,n}$ for different n because the power in different time can be directly controlled by the scaling factors in the time domain.



3.4 Results and Discussions

3.4.1 Computational Complexity

The equalization matrix \mathbf{U}^H is estimated by the use of JD, which has the most computational complexity during the entire equalization procedure stated in Section 3.2.2. JD involves finding an orthonormal matrix via the Jacobi method such that simultaneous diagonalization of a set of square matrices is possible [35]. When an exact solution exists to diagonalize all the matrices in the set, JD can be achieved without errors. Namely, off diagonal elements of the diagonalized matrices are all zeros. When this is not the case, it is always possible to optimize a joint diagonality criterion such that the off diagonal elements of the diagonalized matrices are made as small as possible based on the criterion that is used.

Assumed there is no exact solution, Givens rotation in JD will be repeatedly performed on the set of square matrices until the errors converge. In this case, the computational complexity of JD counted by the number of multiplication is $O(r^2N^3)$, where r is the number of square matrices and N is the size of square matrices .

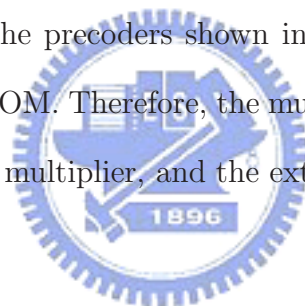
For the precoder-blind equalization scheme, r corresponds to the range of τ in $\mathbf{R}_{\mathbf{z}\mathbf{z}}[\tau]$, and N is the size of $\mathbf{R}_{\mathbf{z}\mathbf{z}}[\tau]$. Without precoder design, the importance of $\mathbf{R}_{\mathbf{z}\mathbf{z}}[\tau]$ is unknown to the receiver. Therefore, a large range for τ is usually required to obtain a good estimate of the equalization matrix [22], which leads to a large value of r . Typically, r falls in the range from 10 to 20, which is comparable to N . Consequently, $O(r^2N^3) \approx O(N^5)$ causes the tremendous computational complexity. However, reducing r is possible by proper design of precoders, which can determine the exact number of correlation matrices that the joint diagonalizer needs to use, which reduces the number of multiplications the receiver needs to perform, thus achieving a lower computational complexity compared to [22] and [21]. As shown in Section 3.4, $r = 2$ is sufficient to achieve a better or comparable BER performance compared with [22] and [21], while the proposed coloring precoders are used. Compared with $O(N^5)$ for the precoder in [22], the computational complexity will then be dramatically reduced since $O(r^2N^3) = O(4N^3) = O(N^3)$ for $r = 2$. For [21], the computational complexity is $O(M^3)$ due to eigenvalue decomposition for solving eigenfilter problems, where M is the IFFT size and usually greater than N . Hence, the proposed precoder-blind equalizer system has a smaller computational complexity compared with both [22] and [21].

3.4.2 Implementation of Precoders by Memory-Based IFFT/FFT

In terms of hardware overhead, the major penalty comes from multiplication of the precoders as illustrated in Figure 3.2. If real-valued multipliers are directly applied before IFFT at the transmitter, the hardware overhead will be proportional to M . The same

situation occurs at the receiver. However, since multiplication due to coloring/decoding can be combined into memory-based IFFT/FFT blocks, this penalty can consequently be eliminated.

A typical memory-based FFT architecture [36] is shown in Figure 3.4, where five dual-ported ($N/4$)-RAMs were employed. The RAM5 is mainly used as a buffer for temporarily storing the computed data. Memory-based FFT architectures generally exploit only one butterfly processing element (or more than one to establish parallelism), some memory blocks to store input or intermediate data, and a control unit to handle read/write operation of memory and data flow direction. In general, memory-based FFT processors can be employed in many applications such as DMT and OFDM based systems. The multiplier in Figure 3.4 multiplies the input data to the FFT coefficients that are stored in ROM. The real-valued coefficients of the precoders shown in (3.23) can be combined with the FFT coefficients and stored in ROM. Therefore, the multiplication with the precoders will be performed using the existing multiplier, and the extra hardware cost can be avoided.



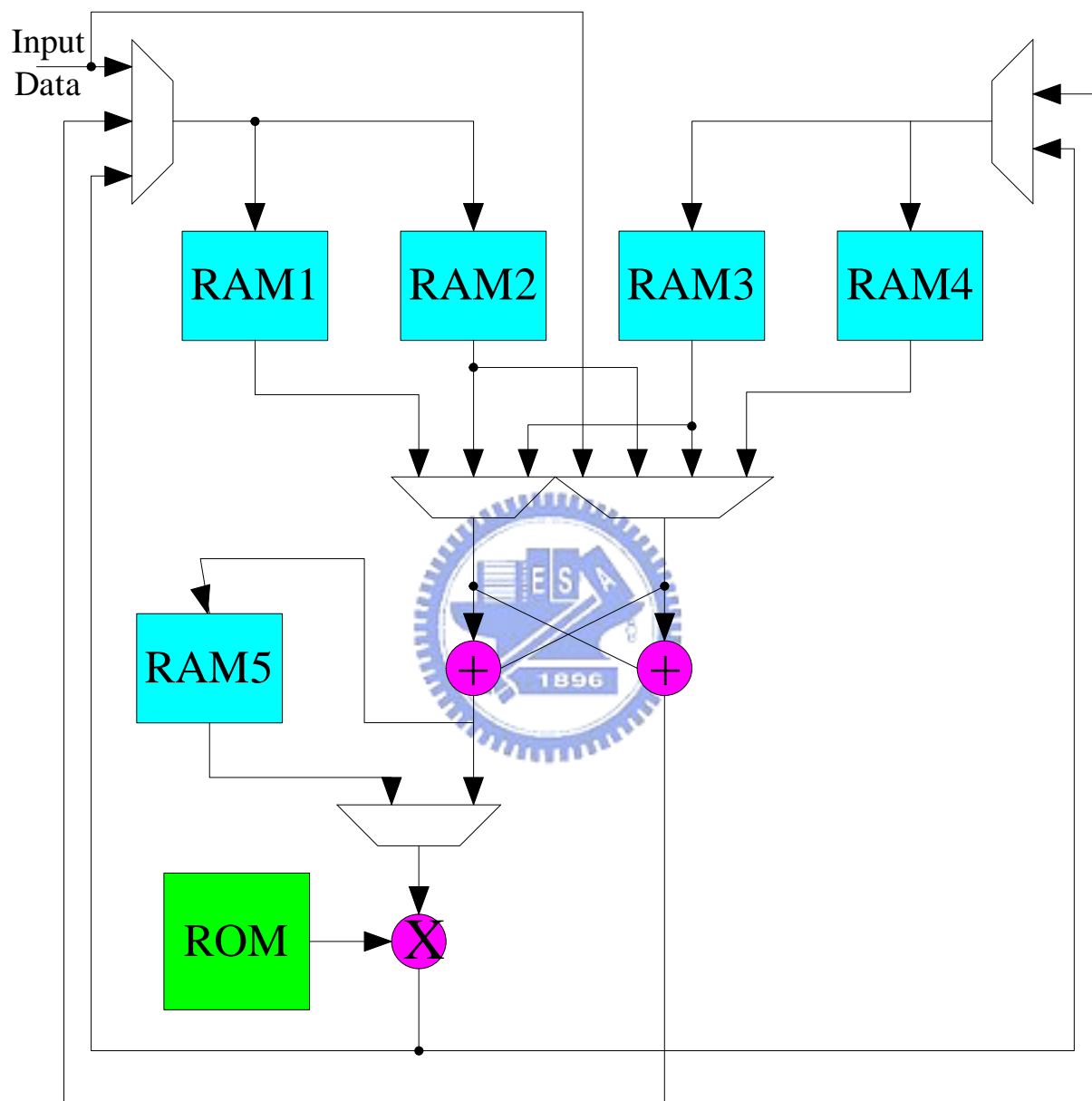


Figure 3.4: A typical memory-based FFT architecture [36].

A MIMO-OFDM system is simulated to evaluate the performance of the proposed scheme. In all simulations, $N_t = 2$, $M = 64$, and $v = 16$. The channels are randomly generated. Two channels were chosen to show the efficacy of the proposed algorithms. The first one is a 3-tap channel with 4 received antennas, i.e. $N_r = 4$, with coefficients

$$\mathbf{H}(z) = \begin{bmatrix} 0.3487 & 0.7220 \\ 0.5121 & 0.5970 \\ -0.3651 & 0.6136 \\ 0.6202 & 0.4880 \end{bmatrix} + \begin{bmatrix} -0.4650 & 0.6189 \\ 0.7682 & -0.3980 \\ -0.9129 & 0.3835 \\ 0.2481 & 0.7807 \end{bmatrix} z^{-1} + \begin{bmatrix} -0.8137 & -0.3094 \\ -0.3841 & 0.6965 \\ 0.1826 & 0.6903 \\ 0.7442 & -0.3904 \end{bmatrix} z^{-2}. \quad (3.26)$$

The second one is a 7-tap channel with 5 received antennas, i.e. $N_r = 5$, with coefficients

$$\mathbf{H}(z) = \begin{bmatrix} 0.5671 & -0.1796 \\ -0.2803 & 0.2466 \\ -0.4485 & 0.2949 \\ -0.4709 & 0.2253 \\ 0.1899 & 0.4222 \end{bmatrix} + \begin{bmatrix} 0.4962 & 0.2694 \\ -0.4484 & 0.3288 \\ 0.1495 & -0.2949 \\ -0.4036 & -0.1931 \\ 0.2279 & 0.3518 \end{bmatrix} z^{-1} + \begin{bmatrix} -0.1418 & 0.2694 \\ -0.5045 & -0.4110 \\ 0.4485 & -0.5160 \\ 0.3363 & 0.4507 \\ 0.6078 & -0.2814 \end{bmatrix} z^{-2} + \begin{bmatrix} -0.3544 & -0.3592 \\ 0.3363 & -0.5754 \\ 0.2242 & -0.1474 \\ -0.4709 & 0.1931 \\ -0.3799 & 0.5629 \end{bmatrix} z^{-3}$$

$$\begin{aligned}
& + \begin{bmatrix} 0.3544 & 0.4490 \\ 0.3363 & 0.1644 \\ -0.2242 & -0.5160 \\ 0.1345 & -0.5151 \\ -0.5318 & -0.2814 \\ -0.2836 & 0.5388 \\ 0.4484 & -0.2466 \\ -0.4485 & -0.3686 \\ 0.4709 & 0.4507 \\ 0.1519 & 0.2111 \end{bmatrix} z^{-4} + \begin{bmatrix} 0.2836 & -0.4490 \\ -0.1962 & -0.4932 \\ -0.5232 & 0.3686 \\ 0.2018 & -0.4507 \\ 0.3039 & -0.4222 \end{bmatrix} z^{-5} \\
& + \begin{bmatrix} -0.2836 & 0.5388 \\ 0.4484 & -0.2466 \\ -0.4485 & -0.3686 \\ 0.4709 & 0.4507 \\ 0.1519 & 0.2111 \end{bmatrix} z^{-6}.
\end{aligned} \tag{3.27}$$

The input data stream to the IFFT at the transmitter is uniformly distributed QPSK signal with zero mean and unit variance. Except for the precoders in Figure 3.11, the precoder used in the simulations is of the form $\alpha_{i,m} = O_i(m)[1 - C_{i,1} \cos(2\pi m/64) - C_{i,2} \cos(4\pi m/64)]$, for $i = 1$ and 2 . That is, $P = 2$. $O_i(m)$ is chosen to make the inner product of the precoder spectrum between two transmit antennas equal to 0. This, however, can easily be generalized to any number of transmit antennas. $C_{i,1}$ and $C_{i,2}$ are set to range from 0.025 to 0.25, and varies for different transmit antennas in order to distinctly color the signal for different transmit antennas. For the simulation results below, $C_{1,1} = 0.25$, $C_{1,2} = 0.025$, $C_{2,1} = 0.175$, and $C_{2,2} = 0.1$. For the scaling factors in the time domain, $\beta_{i,4k} = 1$, $\beta_{i,4k+1} = 0.94$, $\beta_{i,4k+2} = 0.96$, and $\beta_{i,4k+3} = 0.98$ for $k = 0, 1, \dots, 15$.

The spectrum of the coloring precoders is shown in Figure 3.5. The orthogonality generated by $O_i(m)$ between different transmit antennas results in the inner product of zero. Different coefficients are used to induce different temporal correlation for different transmit antennas. In other words, $\tau = 1, 2$ is needed by the joint diagonalizer and has distinct power of autocorrelation functions for both transmit antennas.

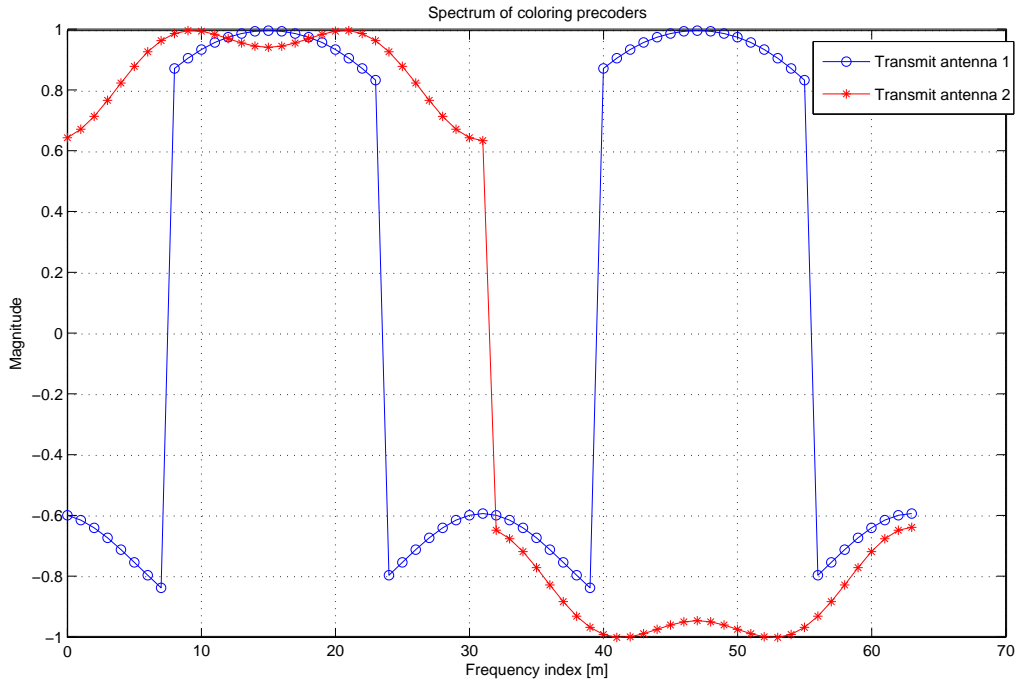


Figure 3.5: Spectrum of the coloring precoders.

3.4.3 BER performance

Figure 3.6 compares the BER performance of the proposed precoder with the JD equalizer with a similar system that uses the JD equalizer but without any precoder. A LS zero-forcing equalizer with CSI is used as benchmark. For the precoder-blind equalizer system, the equalizer uses two correlation matrices, $\mathbf{R}_{\mathbf{z}\mathbf{z}}(\tau_1)$ and $\mathbf{R}_{\mathbf{z}\mathbf{z}}(\tau_2)$, for joint diagonalization. The 3-tap channel in (3.26) was used. Since the input signal $s_{m,\ell}^{(i)}$ is independently distributed, the result reaffirms the idea that if the diagonal entries of the input signal power spectral density matrix are not distinct (no precoder is used), then it is not possible to identify and equalize FIR-MIMO channels using SOS of the received signal. This exhibits a verification of conditions stated in Section 3.1.2 which show that the SOS-based blind equalization can be performed if and only if the system input is colored.

Figure 3.7 shows the BER results of the proposed precoder-equalizer system as the number of OFDM symbols varies for different SNR values. Similar to previous simulations,

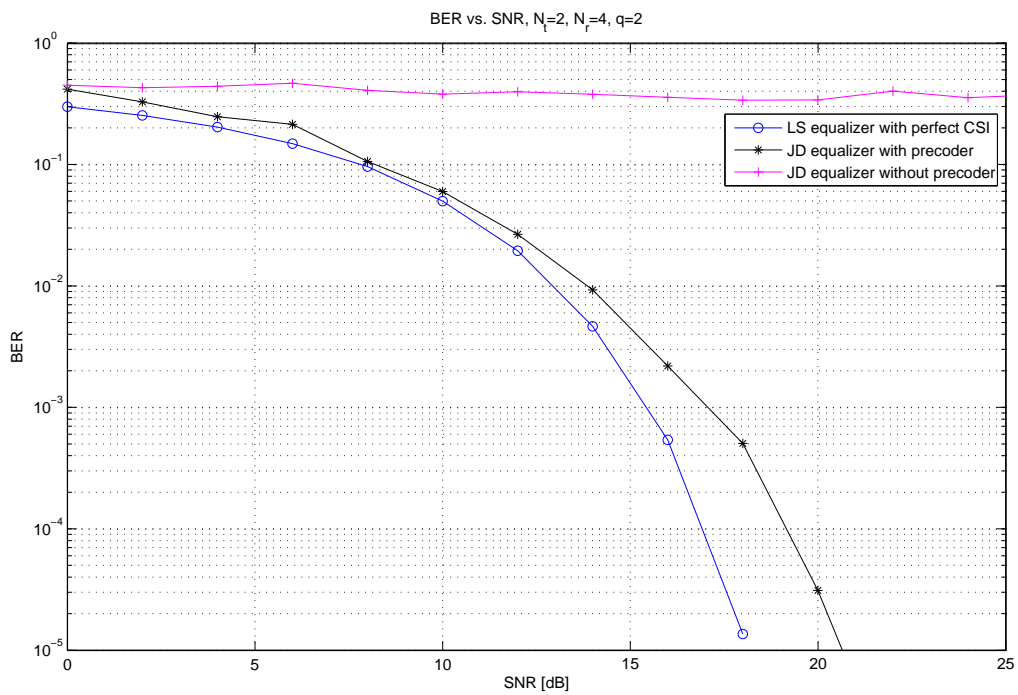


Figure 3.6: Comparison of BER performance between system without coloring and with coloring for 3-tap channel.

$\mathbf{R}_{\tilde{\mathbf{z}}\tilde{\mathbf{z}}}(\tau_1)$ and $\mathbf{R}_{\tilde{\mathbf{z}}\tilde{\mathbf{z}}}(\tau_2)$ are used for joint diagonalization. As the figure shows, the BER of the proposed precoder-equalizer system approaches that of the LS equalizer when the number of symbols increases. This is because as more symbols are used, more accurate estimation of the correlation matrix can be obtained. Furthermore, at SNR = 18 dB, the proposed algorithm is able to equalize the channel using only 350 symbols with a BER of about 10^{-3} . Compare to higher-order statistics techniques such as [10], when the number of symbols needed for equalization is in the order of 10^3 , only a small amount of latency is incurred in the proposed SOS-based technique in order to equalize FIR-MIMO channels.

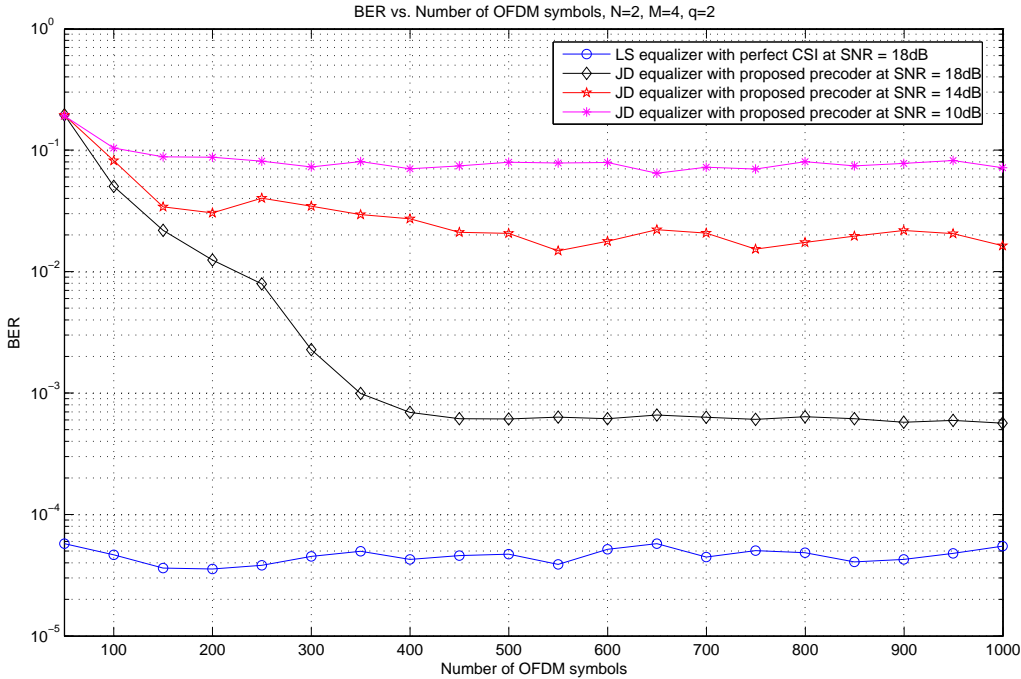


Figure 3.7: BER vs. different number of received OFDM symbols for 3-tap channel at SNR = 10, 14, 18 dB.

Figures 3.8 and 3.9 compare the BER performance of the proposed precoder-blind equalizer system with the precoder-equalizer scheme in [22] and the periodic precoding scheme reviewed in Section 3.2.1 [21]. Results using a LS equalizer and an identical

system that uses no equalization are also shown as benchmarks. As seen in the figures, the performance gap between the LS equalizer and the proposed one remains virtually unchanged as the channel spectrum changes. This shows that the performance of the proposed scheme is insensitive to various channel responses. This can be explained by observing the equation of the precoder in (3.23). Since the precoder is composed of cosine functions, the spectrum of the precoder will fluctuate periodically in the frequency domain. Since the amplitude of the cosine, C_{i,τ_p} , is set to a small value, even if the minimum value of the cosine term coincides with the spectral null of the channel, this will not greatly impact the BER.

Compared with the precoders in [22], the proposed precoders perform better by at least 1 dB in all of the simulated channel conditions. Compared with the periodic precoding scheme in [21], the presented system has a comparable BER performance with the largely diminished latency. Recall the algorithm reviewed in Section 3.2.1 [21], a huge range of lag of cyclic correlation matrix is incurred. Besides, SOS knowledge of the transmitted signal and the received signal are both needed. For $\tilde{\mathbf{R}}_{\mathbf{uu}}[k, \tau]$, a latency of M is incurred since $\tilde{\mathbf{R}}_{\mathbf{uu}}[k, M]$ and $\tilde{\mathbf{R}}_{\mathbf{uu}}[k, -M]$ are required. For $\tilde{\mathbf{R}}_{\mathbf{xx}}[k, \tau]$, $\tilde{\mathbf{R}}_{\mathbf{xx}}[k, -2K - M - q + 3]$ and $\tilde{\mathbf{R}}_{\mathbf{xx}}[k, 2K + M + q - 3]$ induce a latency of $2K + M + q - 3$. To note that the latency of the periodic precoding scheme will increase if the size of IFFT/FFT or channel order increases. Under the conditions of simulation where $M = 64$ and $K = 80$, the latency of the periodic precoding scheme is $q + 221$ which is a relatively huge number while the proposed precoder-equalizer system has a small latency from $\tau_2 = 2$. The latency of the proposed precoder-blind system is dictated by the precoder design and independent of IFFT/FFT size. A comparison to both [22] and [21] is summarized in Table 3.4. Recall that M is the IFFT size, v is the length of CP, q is the channel order, and N is the size of correlation matrices of the whitened signal.

Figure 3.10 shows the BER result when different lags are chosen for joint diagonaliza-

Table 3.4: Performance comparison

Performance Indices	Proposed Precoder-Blind System	Periodic Precoder System [21]	Using Precoder in [22]
SNR at BER = 10^{-4} for 3-tap channel	19.5 dB	19 dB	21 dB
Number of symbols for SOS at SNR=18 dB	350	500	350
Latency from correlation matrix	Controlled by precoders	$3M + 2v + q - 3$	$10 \sim 20$
Computational Complexity	$O(N^3)$	$O(M^3)$	$O(N^5)$

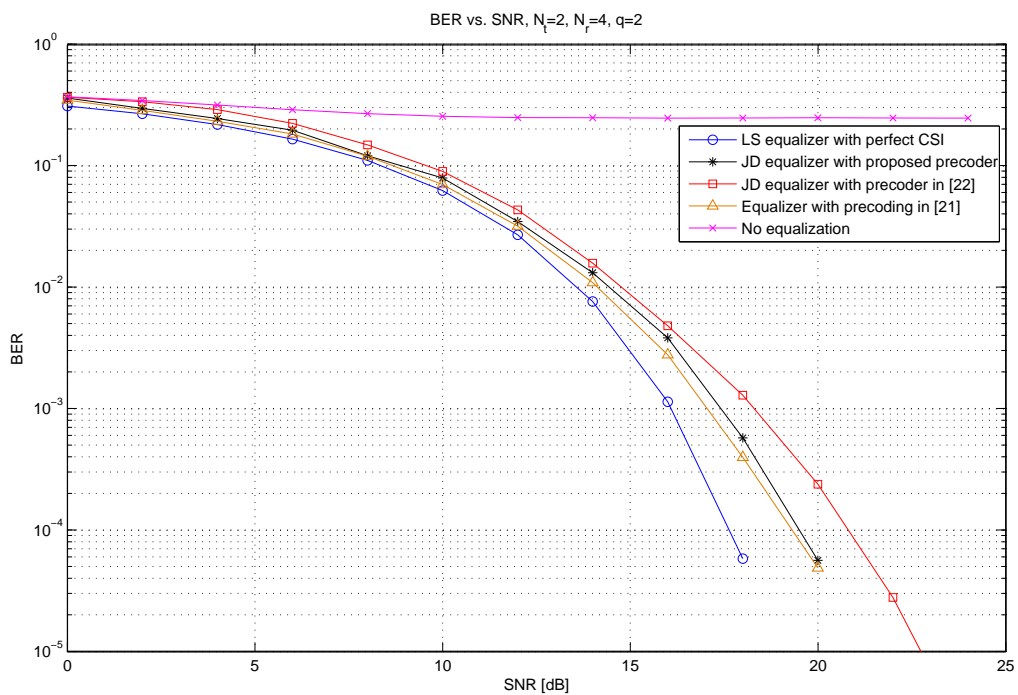


Figure 3.8: Comparison of BER vs. SNR with different algorithms for 3-tap channel.

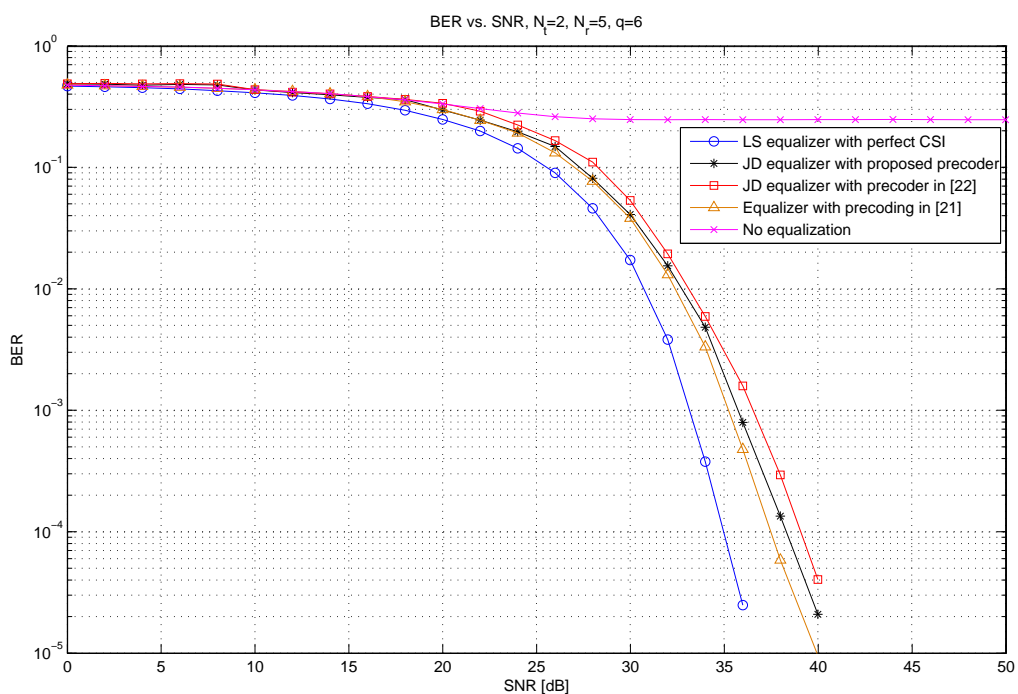


Figure 3.9: Comparison of BER vs. SNR with different algorithms for 7-tap channel.

tion at the receiver. As explained in Section 3.2.2, if $\tau_1 = 1$ and $\tau_2 = 2$, then $\mathbf{R}_{\mathbf{z}\mathbf{z}}(1)$ and $\mathbf{R}_{\mathbf{z}\mathbf{z}}(2)$ become the only correlation matrices that are needed for joint diagonalization. This is reaffirmed by the simulation results in Figure 3.10 when the best BER performance is attained when only $\mathbf{R}_{\mathbf{z}\mathbf{z}}(1)$ and $\mathbf{R}_{\mathbf{z}\mathbf{z}}(2)$ are used for equalization. When other correlation matrices are used, the BER curves saturate to a noise floor. Since the choice for τ_p is chosen at the transmitter and it determines exactly which, as well as how many, correlation matrices should be used at the receiver for equalization, the transmitter has complete control on the computational complexity of the equalizer.

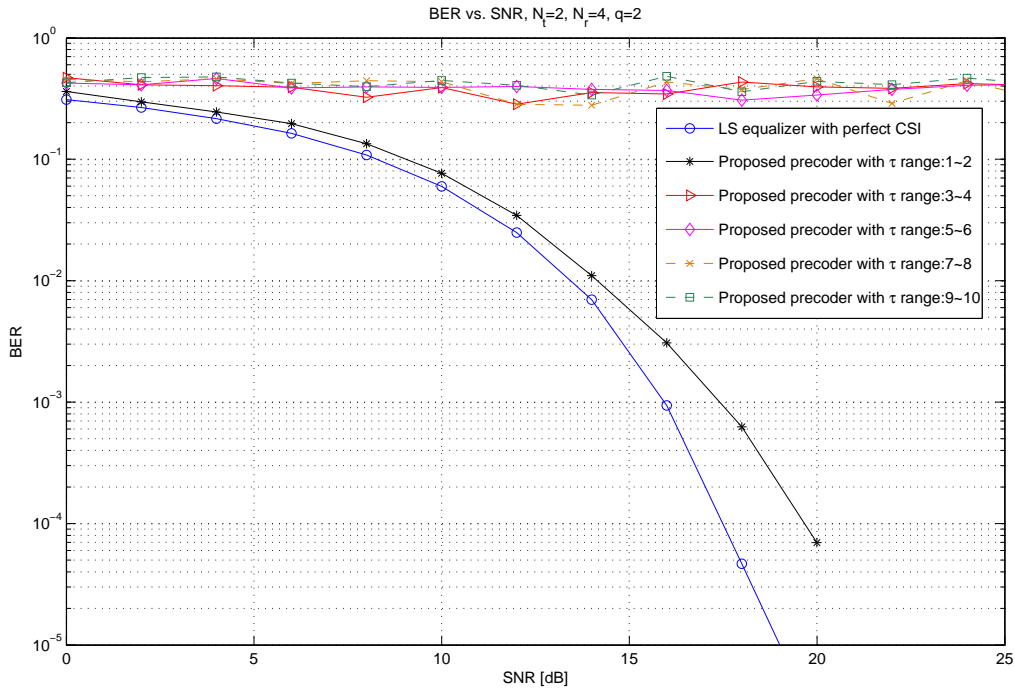


Figure 3.10: BER vs. SNR with different lag for 3-tap channel.

As discussed earlier, the design parameter P cannot be increased indefinitely in order to enhance equalization performance at the expense of increase computational complexity. Likewise, P also cannot be made too small since it will adversely affect the equalization performance. Figure 3.11 shows the result of the proposed algorithm when P is allowed to vary from 1 to 5. As seen from the figure, the BER is smallest when $P = 2$. Therefore,

P cannot be made arbitrary small in order to minimize computational complexity at the receiver, but it also cannot be made arbitrarily big since it will adversely impact the BER performance since this will induce too much amplitude variation into the transmitted bitstream.

Amplitude variation is dominated by not only P but also coefficients of the precoder. Obviously, larger coefficients lead to more amplitude variation of the spectrum. To discuss the effects the coefficients of the precoder have on the BER performance, we define a ratio $\gamma = \kappa/\mu$, where κ is the absolute value of the maximum coefficient and μ is the absolute value of the minimum coefficient. When P is fixed, a large γ induces more amplitude variation. Figure 3.12 shows the BER performance under distinct values of γ . This is obtained by varying κ while μ is held constant. It can be seen that the best BER occurs when $\gamma = 10$, and the BER will become worse no matter if γ is larger or smaller than 10. Among all the values that have been tested, $\gamma = 16$ gives the worst BER because it induces too much amplitude variation into the transmitted signal. This implies that there exists an optimal choice for the precoder coefficients. If the magnitude of the coefficients is too small, then the accuracy of the estimates of \mathbf{U} is not sufficient. If the magnitude is too large, then too much amplitude variation is introduced in the spectrum such that the BER will degrade. Hence, the effect of γ is similar to that of P .

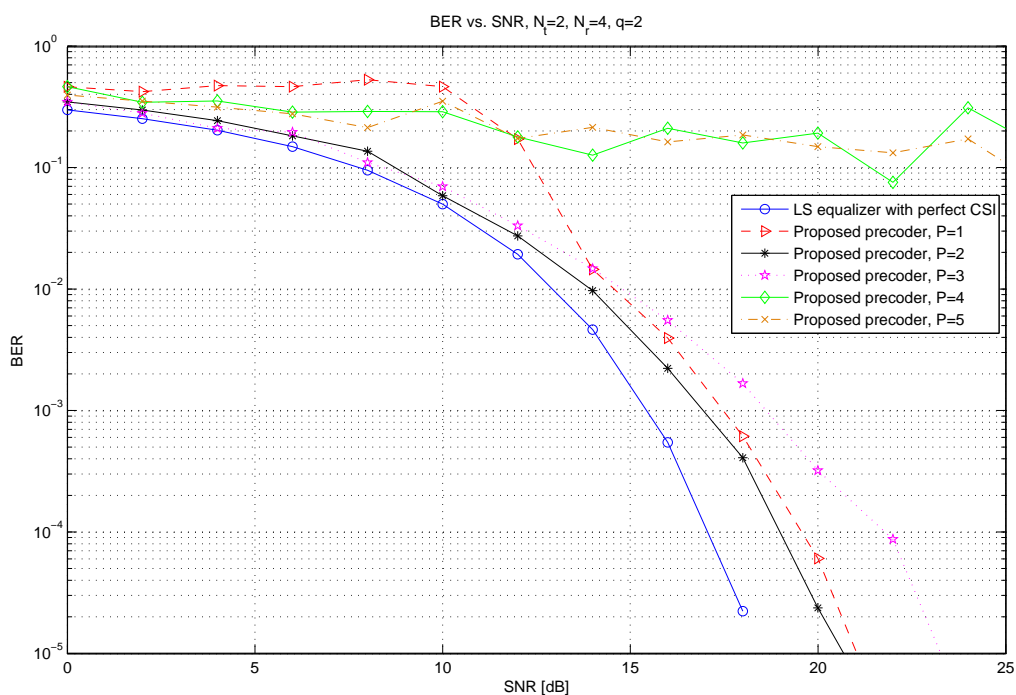


Figure 3.11: BER vs. SNR with different P for 3-tap channel.

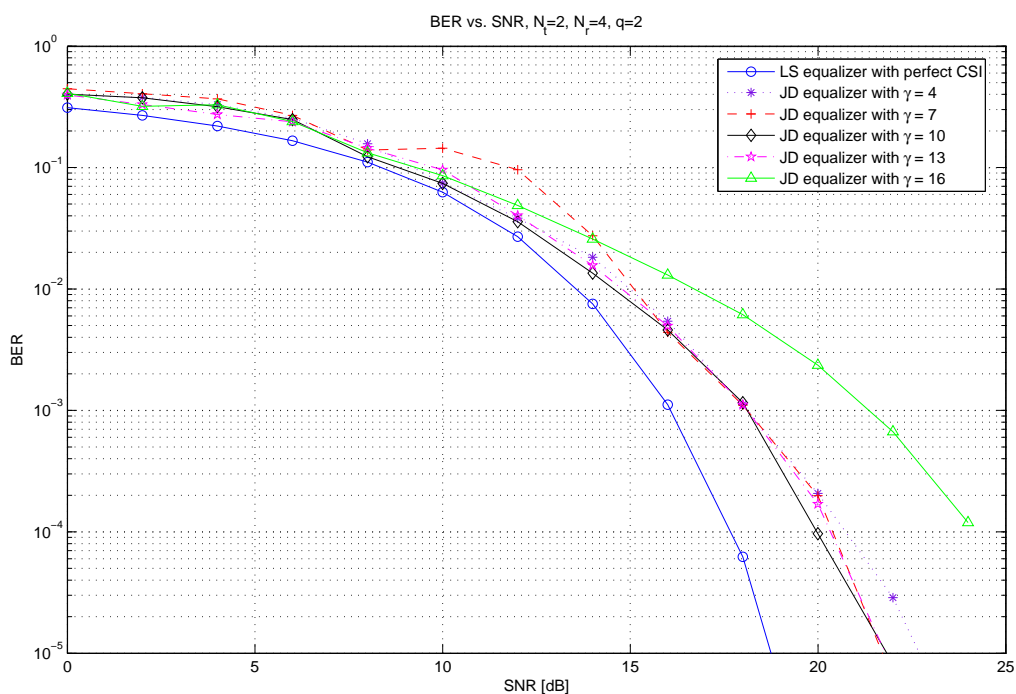
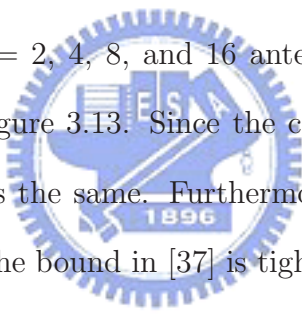


Figure 3.12: BER vs. SNR with different γ for 3-tap channel.

3.4.4 Channel Capacity

The channel capacity of the precoder-blind system is discussed under a Rayleigh block flat fading channel [37]. We assume that $N_t = N_r = N$. The total power of all transmit antennas is denoted by P_{tx} . Assumed P_{tx} is uniformly allocated by all transmit antennas, each transmit antenna then has a power of P_{tx}/N .

Figure 3.13 shows the capacity vs. the number of antennas with SNR varying between 0 and 30 dB. It is clear that the capacity increases linearly with the number of antennas and logarithmically with SNR. For SNR = 10 dB and $N = 10$, the simulated average capacity is 27.1485 bits/s/Hz. Figure 3.14 shows the capacity per antenna vs. SNR with various N . The capacity per antenna is the total capacity normalized with respect to N . Bound limit refers to the theoretical lower bound of the capacity per antenna where $N = 2$ [37]. The curves for $N = 2, 4, 8,$ and 16 antennas coincide as shown in Figure 3.14. This is consistent with Figure 3.13. Since the capacity increases linearly with N , the normalized capacity remains the same. Furthermore, these curves are very close to the bound. This confirms that the bound in [37] is tight and can be used to estimate the channel capacity.



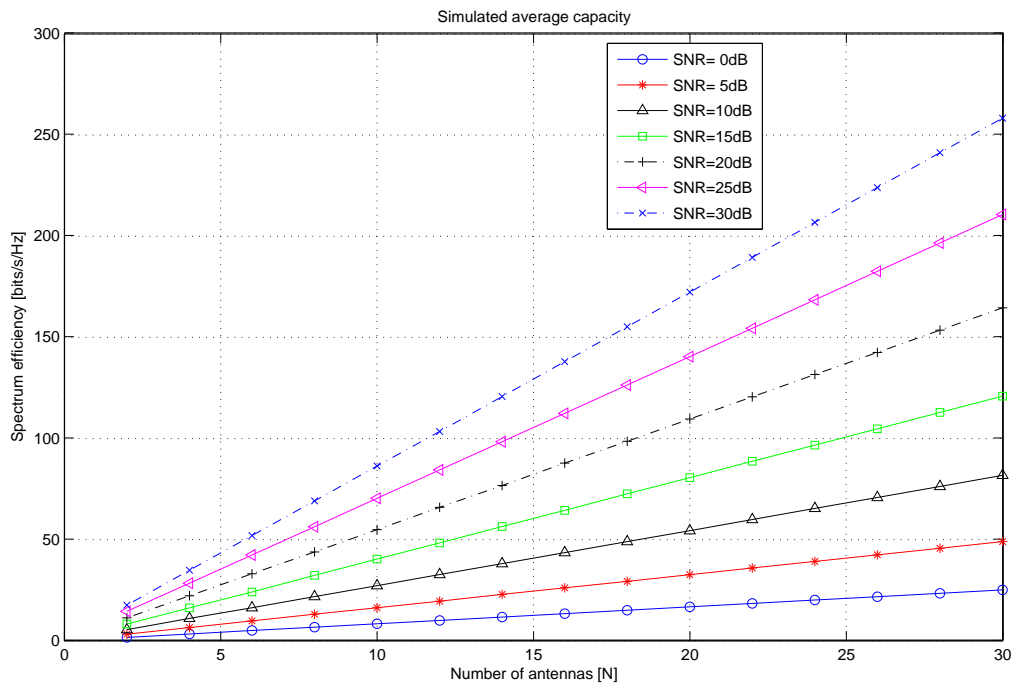


Figure 3.13: Capacity vs. Number of antennas with different SNR.

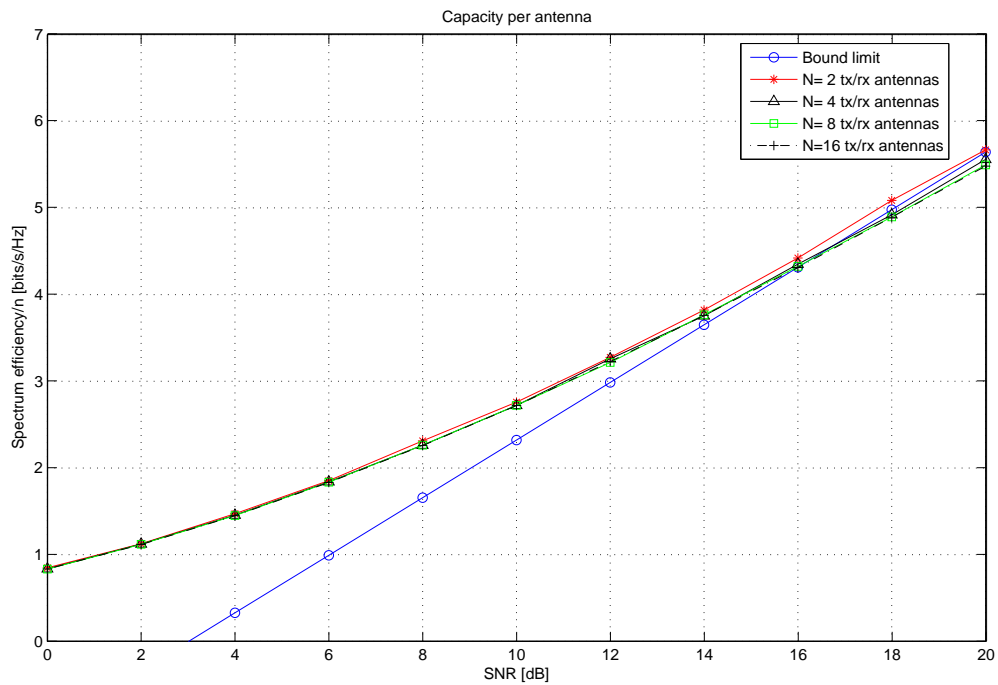


Figure 3.14: Capacity per n vs. SNR with different n .

Chapter 4

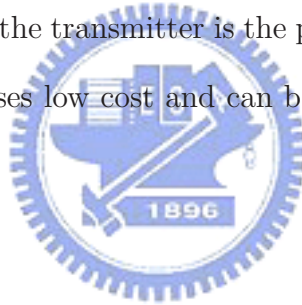
Conclusion and Future Work

4.1 Conclusion

A SOS-based precoder-blind equalizer system has been proposed to equalize FIR-MIMO channels for MIMO-OFDM systems, which consists of coloring precoders at the transmitter, correlation estimation, whitening process, JD, and decoloring decoders at the receiver. The coloring precoders inject temporal correlation into the transmitted signal in order to satisfy the blind channel identifiability conditions stated in Section 3.1.1. In addition, the proposed design also supports the equalizability conditions stated in Section 3.1.2, which allow for direct equalization of FIR-MIMO channels using SOS of the received signal. As stated earlier, this has an advantage over traditional two-step equalization methods because those algorithms will likely result in suboptimal equalizers.

Simulation results have shown that using the proposed precoder cannot only outperform the precoder proposed in [22] in terms of BER, but also allows the transmitter to dictate which, and how many, correlation matrices are to be used for equalization at the receiver. This decreases the amount of computational complexity at the receiver compared to the scheme in [22] since the number of correlation matrices needed for JD can be predetermined before transmission. Moreover, the proposed scheme also has much

lower latency than a similar scheme in [21]. This is because the range of lag for correlation matrices can be determined at the transmitter and it is independent of the FFT size. In terms of BER, an optimal choice for amplitude variation from coloring exists. If amplitude variation is too little, the accuracy of the estimates of \mathbf{U} is not sufficient. However, the BER is also degraded if too much amplitude variation is introduced. Thus, coloring of the transmitted signal is essential to SOS based blind equalization, but the coloring process cannot introduce too much amplitude variation into the signal because it will severely degrade the BER. In addition to BER performance, we have show that by using our proposed precoder-blind equalizer system, we can achieve a spectrum efficiency about 25 bits/s/Hz for a 10×10 system. We have also shown that the spectrum efficiency for our system is close to the theoretical bound stated in [37] when $N_t = 2$. Furthermore, the hardware overhead at the transmitter is the precoder involving with real-valued multiplication only, which imposes low cost and can be incorporated into memory-based IFFT/FFT in advance.



4.2 Future Work

In the future, a semi-blind equalization scheme can be extended from this work. High spectrum efficiency and channel capacity can be achieved by blind techniques. However, the BER loss compared with non-blind algorithms is an obstacle to practical application. To mitigate the BER, a short training sequence can be introduced to constitute a semi-blind system, which has better BER performance than blind systems while its channel capacity is still higher than that of non-blind systems. Moreover, SBTC or orthogonal STBC can be taken into account since these coding algorithms are often used to increase transmit diversity for a reliable link of MIMO systems. It is also possible to combine coloring precoders with precoders of multi-user MIMO systems.

Bibliography

- [1] Bingham, J.A.C., “Multicarrier Modulation for Data Transmission: An Idea Whose Time Has Come,” *Communications Magazine, IEEE*, vol. 28(5), pp. 5–14, May 1990.
- [2] Gesbert D., Shafi M., Da-shan Shiu, Smith P.J. and Naguib A., “From Theory to Practice: An Overview of MIMO Space-Time Coded Wireless Systems,” *IEEE Journal on Selected Areas in Communications*, vol. 21(3), pp. 281–302, Apr. 2003.
- [3] Paulraj A.J., Gore D.A., Nabar R.U. and Boleskei H., “An Overview of MIMO Communications - A Key to Gigabit Wireless,” *Proceedings of the IEEE*, vol. 92(2), pp. 198–218, Feb. 2004.
- [4] Wolniansky P.W., Foschini G.J., Golden G.D., Valenzuela R.A., Lucent Technol and Holmdel NJ, “V-BLAST: An Architecture for Realizing Very High Data Rates over The Rich-Scattering Wireless Channel,” *International Symposium on Signals, Systems, and Electronics*, pp. 295–300, Oct. 1998.
- [5] Mai Vu and Paulraj A., “MIMO Wireless Linear Precoding,” *Signal Processing Magazine, IEEE*, vol. 24(5), pp. 86–105, Sep. 2007.
- [6] Hongwei Yang, “A Road to Future Broadband Wireless Access: MIMO-OFDM-Based Air Interface,” *Communications Magazine, IEEE*, vol. 43(1), pp. 53–60, Jan. 2005.

- [7] Mach P. and Bestak R., “WiMAX Performance Evaluation,” *Sixth International Conference on Networking*, pp. 17–20, Apr. 2007.
- [8] A. Lozano, F.R. Farrokhi and R.A. Valenzuela, “Lifting the Limits on High-Speed Wireless Data Access Using Antenna Arrays,” *IEEE Communications Magazine*, vol. 39(9), pp. 156–162, Sep. 2001.
- [9] G.J. Foschini, “Layered Space-Time Architecture for Wireless Communication in a Fading Environment When using Multi-Element Antennas,” *Bell Labs Technical Journal*, vol. 1(2), pp. 41–59, Aug. 1996.
- [10] G.B. Giannakis, “Identification of Nonminimum Phase Systems Using Higher Order Statistics,” *IEEE Trans. on Acoustics, Speech, and Signal Processing*, vol. 37(3), pp. 360–378, Mar. 1989.
- [11] J.M. Mendel, “Tutorial on Higher-Order Statistics (Spectra) in Signal Processing and System Theory: Theoretical Results and Some Applications,” *Proc. of the IEEE*, vol. 79(3), pp. 277–305, Mar. 1991.
- [12] L. Tong, G. Xu and T. Kailath, “Blind Identification and Equalization Based on Second-Order Statistics: A Time Domain Approach,” *IEEE Trans. on Information Theory*, vol. 40(2), pp. 340–349, Mar. 1994.
- [13] H. Liu, G. Xu and L. Tong, “A Deterministic Approach to Blind Identification of Multi-Channel FIR Systems,” in *Proc. of the Intl. Conf. on Acoustics, Speech, and Signal Processing*, vol. 4, Apr. 1994, pp. 581–584.
- [14] E. Moulines, P. Duhamel, J.F. Cardoso and S. Mayrague, “Subspace Methods for the Blind Identification of Multichannel FIR Filters,” *IEEE Trans. on Signal Processing*, vol. 43(2), pp. 516–525, Feb. 1995.

- [15] A. Gorokhov and P. Loubaton, "Subspace-Based Techniques for Blind Separation of Convolutive Mixtures with Temporally Correlated Sources," *IEEE Trans. on Circuits and Systems – I: Fundamental Theory and Applications*, vol. 44(9), pp. 813–820, Sep. 1997.
- [16] K. Abed-Meraim and Y. Hua, "Blind Identification of Multi-Input Multi-Output System Using Minimum Noise Subspace," *IEEE Trans. on Signal Processing*, vol. 45(1), pp. 254–258, Jan. 1997.
- [17] T. Kailath, *Linear Systems*. Prentice-Hall, 1980.
- [18] Y. Hua and J.K. Tugnait, "Blind Identifiability of FIR-MIMO Systems with Colored Input Using Second Order Statistics," *IEEE Signal Processing Letters*, vol. 7(12), pp. 348–350, Dec. 2000.
- [19] Y. Hua, S. An and Y. Xiang, "Blind Identification of FIR MIMO Channels by Decorrelating Subchannels," *IEEE Trans. on Signal Processing*, vol. 51(5), pp. 1143–1155, May 2003.
- [20] A. Belouchrani, K. Abed-Meraim, J.-F. Cardoso and E. Moulines, "A Blind Source Separation Technique Using Second-Order Statistics," *IEEE Trans. on Signal Processing*, vol. 45(2), pp. 434–444, Feb. 1997.
- [21] H. Bolcskei, R.W. Heath and A.J. Paulraj, "Blind Channel Identification and Equalization in OFDM-Based Multiantenna Systems," *IEEE Trans. on Signal Processing*, vol. 50(1), pp. 96–109, Jan. 2002.
- [22] C.C. Fung, M.W. Kwan and C.W. Kok, "Second-Order Statistics Based Minimal Transmit Redundancy Space-Time FIR Precoder-Blind Equalizer," *Proc. of the Asilomar Conference on Signals, Systems and Computers*, pp. 1019–1023, Oct. 2005.

- [23] Shang-Kang Deng and Mao-Chao Lin, “OFDM PAPR reduction using clipping with distortion control,” in *IEEE International Conference on Communications*, vol. 4, May 2005, pp. 2563–2567.
- [24] D. R. Company, *Using MIMO-OFDM technology to Boost Wireless LAN Performance Today*. St. Louis: White Paper, 2005.
- [25] J.G. Proakis, *Digital Communications*. McGRAW-HILL, 2001.
- [26] V. Tarokh, N.Seshadri and A. Calderbank, “Space-Time Codes for High Data Rate Wireless Communication: Performance Criterion and Code Construction,” *IEEE Trans. on Inform. Theory*, vol. 44(2), pp. 744–765, Mar. 1998.
- [27] Lizhong Zheng and Tse D.N.C, “Diversity and Multiplexing: A Fundamental Trade-off in Multiple-Antenna Channels,” *IEEE Trans. on Inform. Theory*, vol. 49(5), pp. 1073–1096, May 2003.
- [28] En Zhou, Xing Zhang, Hui Zhao and Wenbo Wang, “Synchronization Algorithms for MIMO OFDM Systems,” in *WCNC of IEEE Communications Society*, vol. 1, Mar. 2005, pp. 18–22.
- [29] Perels D., Studer C. and Fichtner W., “Implementation of a Low-Complexity Frame-Start Detection Algorithm for MIMO Systems,” in *IEEE International Symposium on Circuits and Systems*, May 2007, pp. 1903–1906.
- [30] Schenk T.C.W. and van Zelst A., “Frequency Synchronization for MIMO OFDM Wireless LAN Systems,” in *IEEE 58th Vehicular Technology Conference*, vol. 2, Oct. 2003, pp. 781–785.
- [31] Yujiro Inouye and Ruey-Wen Liu, “A System-Theoretic Foundation for Blind Equalization of an FIR MIMO Channel System,” *IEEE Trans. on Circuits and Systems*, vol. 49(4), pp. 425–436, Apr. 2002.

- [32] R.-W. Liu, Y. Inouye and H. Luo, “A System-Theoretic Foudation for Blind Signal Separation of MIMO-FIR Convolutive Mixtures - A Review,” in *Proc. of the Independent Component Analysis Conference*, Jun. 2000, pp. 205–210.
- [33] R. W. Heath, Jr and G. B. Giannakis, “Exploiting Input Cyclostationarity for Blind Channel Identification in OFDM Systems,” *IEEE Trans. on Signal Processing*, vol. 47, pp. 848–856, Mar. 1999.
- [34] H. Bolcskei, P. Duhamel and R. Hleiss, “A Subspace-Based Approach to Blind Channel Identification in Pulse Shaping OFDM/OQAM Systems,” *IEEE Trans. on Signal Processing*, vol. 49, pp. 1594–1598, July 2001.
- [35] Jean-Francois Cardoso and Antoine Souloumiac, “Jacobi Angles for Simultaneous Diagonalization,” *Society for Industrial and Applied Mathematics on Matrix Analysis and Applications*, vol. 17(1), pp. 161–164, Jan. 1996.
- [36] C. K. Chang, C. P. Hung and S. G. Chen, “An Efficient Memory-Based FFT Architecture,” in *Proc. of IEEE International Symposiums on Circuits and Systems*, vol. 2, 2003, pp. 129–132.
- [37] B. Vucetic and J. Yuan, *Space-Time Coding*. Australia: Wiley, 2003.